α-Helix C-Terminus Can Act as a Relay to Mediate Long-range Hole-Migration in Proteins

Xiaohua Chen[†], Laibin Zhang[†], Liang Zhang[†], Wenming Sun[†], Zhenwei Zhang[†], Haiying Liu[†], Yuxiang Bu[1,†], and Robert I. Cukier [1,‡]

The Center for Modeling & Simulation Chemistry, Institute of Theoretical Chemistry, Shandong University, Jinan 250100, P. R. China and Department of Chemistry, Michigan State University, East Lansing, MI 48824-1322

Supporting Information

Contents for Supplementary Materials

[1] *The corresponding authors: Yuxian Bu, byx@sdu.edu.cn; Robert I. Cukier, cukier@chemistry.msu.edu*
[†] *Shandong University*
[‡] *Michigan State University*

1. Calculational Details

All calculations were carried out by using Gaussian 03 suite of programs.[S1] The UB3LYP[S2] hybrid functional in conjunction with the 6-31G(d) basis set[S3,S4] was utilized to optimize the geometries of all the helixes (including neutral molecules and radical cations) and to perform the harmonic vibrational analyses for confirming minima (all real frequencies). More accurate methods B3LYP/6-31++G(d,p), and MP2/6-31G(d) were also used to verify the reliability of 6-31G(d) upon the properties of α-$(G)_6$ and α-$(G)_6^{\bullet+}$. To obtain more accurate ionization energies, single-point energies were recalculated for all the helical radical cations and the corresponding neutral helices (the same structure as cation) at the B3LYP/6-31++G(d,p)//B3LYP/6-31G(d) level of theory. The vertical ionization potential (IPv) was calculated as the energy difference between the neutral and cationic species at the geometry of optimized neutral helix. The adiabatic ionization potential (IP_A) was defined as the energy difference between the neutral molecule and the corresponding cation at their respective relaxed helical geometries. Besides, the restricted molecular orbital contours were used to display the orbital character.

In addition, dielectric continuum theories[S5,S6] were used to determine the position of electron hole, ionization potential, and dipole movement of helix. However, the dielectric constant of proteins could not be accurately measured because of the complexity of protein structures. It was proposed the protein dielectric constant could vary from as little as 2 in the protein center to values of 25 or more (78.36) in the polar outer region, with intermediate values in certain specific regions.[S7-S10] So all the helixes were carried out single-point calculations in different continuum solvents, including water (ε=78.36) and benzene (ε=2.247), at the B3LYP/6-31++G(d,p) level of theory by means of the polarizable continuum model (PCM)[S11].

(S1) Frisch, M. J.; Trucks, G. W.; Schlegel, H. B.; Scuseria, G. E.; Robb, M. A.; Cheeseman, J. R.; Montgomery, Jr., J. A.; Vreven, T.; Kudin, K. N.; Burant, J. C.; Millam, J. M.; Iyengar, S. S.; Tomasi, J.; Barone, V.; Mennucci, B.; Cossi, M.; Scalmani, G.; Rega, N.; Petersson, G. A.; Nakatsuji, H.; Hada, M.; Ehara, M.; Toyota, K.; Fukuda, R.; Hasegawa, J.; Ishida, M.; Nakajima, T.; Honda, Y.; Kitao, O.; Nakai, H.; Klene, M.; Li, X.; Knox, J. E.; Hratchian, H. P.; Cross, J. B.; Bakken, V.; Adamo, C.; Jaramillo, J.; Gomperts, R.; Stratmann, R. E.; Yazyev, O.; Austin, A. J.; Cammi, R.; Pomelli, C.; Ochterski, J. W.; Ayala, P. Y.; Morokuma, K.; Voth, G. A.; Salvador, P.;

Dannenberg, J. J.; Zakrzewski, V. G.; Dapprich, S.; Daniels, A. D.; Strain, M. C.; Farkas, O.; Malick, D. K.; Rabuck, A. D.; Raghavachari, K.; Foresman, J. B.; Ortiz, J. V.; Cui, Q.; Baboul, A. G.; Clifford, S.; Cioslowski, J.; Stefanov, B. B.; Liu, G.; Liashenko, A.; Piskorz, P.; Komaromi, I.; Martin, R. L.; Fox, D. J.; Keith, T.; Al-Laham, M. A.; Peng, C. Y.; Nanayakkara, A.; Challacombe, M.; Gill, P. M. W.; Johnson, B.; Chen, W.; Wong, M. W.; Gonzalez, C.; and Pople, J. A. Gaussian 03, Revision C.02; Gaussian, Inc.: Wallingford, CT, 2004.

(S2) (a) Becke, A. D. *J. Chem. Phys.* **1993**, *98*, 5648–5652. (b) Lee, C.; Yang, W.; Parr, R. G. *Phys. Rev. B* **1988**, *37*, 785–789.

(S3) Wu, Y.; Zhao, Y. A *J. Am. Chem. Soc.* **2001**, *123*, 5313-5319.

(S4) Topol, I. A.; Burt, S. K.; Deretey, E.; Tang, T.; Perczel, A. Rashin, A.; Csizmadia, I. G. *J. Am. Chem. Soc.* **2001**, *123*, 6054–6060.

(S5) Cramer, C. J.; Truhlar, D. G. *Chem. Rev.* **1999**, *99*, 2161–2200.

(S6) Tomasi, J.; Persico, M. *Chem. Rev.* **1994**, *94*, 2027–2094.

(S7) King, G.; Lee, F.; Warshel, A. *J. Chem. Phys.* **1991**, *95*, 4366-4377.

(S8) Smith, P.; Brunne, R.; Mark, A.; van Gunsteren, W. *J. Phys. Chem.* **1993**, *97*, 2009-2014.

(S9) Simonson, T.; Perahia, D. *Proc. Natl. Acad. Sci. U.S.A.* **1995**, *92*, 1082-1086.

(S10) Simonson, T.; Brooks III, C. L. *J. Am. Chem. Soc.* **1996,** *118,* 8452-8458.

(S11) (a) Cancès, M. T.; Mennucci, B.; Tomasi, J. *J. Chem. Phys.* **1997**, *107*, 3032-3041. (b) Mennucci, B. Tomasi, J. *J. Chem. Phys.* **1997**, *106*, 5151-5155. (c) Cossi, M.; Barone, V.; Mennucci, B.; Tomasi, J. *Chem. Phys. Lett.* **1998**, *286*, 253-263. (d) Tomasi, J.; Mennucci, B.; Cammi, R. *Chem. Rev.* **2005**, *105*, 2999–3094.

2. Some Additional Remarks

a) *Regarding Ionization Potentials (IP) Used as an Indirect Quantity to Scale the Ability of a Species in Releasing an Electron or Accepting a Hole*.

We use ionization potentials (IP) as a measure to analyze the possibility of hole formation in the helices. Although IP is not a direct indicator for a hole-relay energy scale in hole migration, it exactly reflects the ability of electron loss of a donor, or a relay element, and thus can be viewed as an indirect measure. IPs and standard oxidation potentials are two different physical quantities. However, they are inherently correlated, both reflecting the ability of a species to be oxidized (to inject a hole). As a general trend, if the IP of a species is high, it does not qualify as an electron donor. This suggests that it is difficult for a hole to reside there; thus, it is not a good hole relay element. Of course, in a real hole migration process, whether or not a redox reaction (that is, an electron/hole transfer reaction) can proceed depends on the relative oxidation ability of an oxidant. That is, a difference of IP (electron donor) and electron affinity (EA, electron acceptor=oxidant, which for an adiabatic EA equals the adiabatic IP of the reduced oxidant). Clearly, a relation is still available by replacing IP by redox potential. Actually, as commonly done, the IP can also be related to the electron transfer (ET) energetics. According to Marcus ET theory, the ET activation energy (ΔE) can be expressed as

$$\Delta E = (\lambda+\Delta E_0)^2/4\lambda$$

ΔE_0 is the reaction heat, the ET driving force, and λ is the reorganization energy of the reactive system, and can be further expressed as

$$\lambda = \lambda_{donor} + \lambda_{acceptor} = (IP_v - IP_a)_{donor} + (EA_v - EA_a)_{acceptor}$$

In this equation, IP_v denotes the vertical IP, while IP_a denotes the adiabatic one. The same is true for the EA (electron affinity). Inherently, EA_v and EA_a of a species (A) are closely related to the IPs of its corresponding reduced form (A^-), for example, $IP_a(A^-) = EA_a(A)$. Therefore, IPs are closely related to the ET energetics. In an actual ET process there is no need for the transferring electron to escape from a donor with the IP-based energy and then to add to an acceptor with the EA-based energy. That is, most biological electron flow occurs at potentials far lower than the IP required to oxidize a donor (e.g. Trp). IPs really reflect the ability of a species to release or accept an electron

in an ET process. Two important facts that support this view are that the IP of Trp is the smallest among all amino residue side groups, while the cation-radicals of Trp can be found frequently in proteins due to radiation-induced damages. Furthermore, the two most easily oxidized side chains of aromatic amino-acid residues, Trp and Try, have been shown by experiment to be involved in a number of important biological electron transfer processes (Bu, et al *JPC B* **2009**,*113*,16681 and references therein), such as DNA photolyase (Aubert, et al. *PNAS* **1999**, *96*, 5423), bovine serum albumin (Mukherjee, et al. *Biophys. Chem.* **2003**,*103*,89), hen egg-white lysozyme (Weinstein, et al. *BBA* **1991**,*1076*,173; Bobrowski, et al. *Biophys. Chem.* **1997**,*63*,153), *E. coli* ribonucleotide reductase (Bollinger, et al. *JACS* **1994**,*116*,8024; Reece, et al. *BBA* **2005**,*1706*,232), nitrite reductase in *Achromobacter cycloclastes* (Zumft, *Microbiol. Mol. Biol. Rev.* **1997**,*61*,533; Yamaguchi, et al *Biochem. Biophys. Res. Commun.* **2005**,*336*,210). For example, **i**) ET from Tyr to a Trp radical was demonstrated to be an essential step in the process leading to the active form of photolyase in *Anacystis nidulans* (Aubert, et al. *PNAS* **1999**,*96*, 5423), and a three-Trp chain (Trp390, Trp367, Trp314) was proposed as a relay for charge hopping migration (Sancar *Chem. Rev.* **2003**,*103*,2203; Aubert, et al *JACS* **1999**,*121*, 8659; Reece, et al *Phil. Trans. R. Soc. B* **2006**,*361*,1351). **ii**) In the R2 subunit of *E. coli* ribonucleotide reductase, ET from Trp48 to Tyr122 radical cation is the first step, and that from Tyr356 to Trp48 is the second step, in this 35 Å, long range electron transport chain (Bollinger, et al *JACS* **1994**,*116*,8024; Sancar, *Chem. Rev.* **2003**,*103*,2203; Aubert, et al *JACS* **1999**,*121*,8659; Reece, et al *Phil. Trans. R. Soc. B* **2006**,*361*,1351; Sneeden, et al *JBC* **2004**,*279*,40723; Baldwin, et al *JACS* **2000**,*122*,12195; Bollinger, et al *JACS* **1994**,*116*,8015). **iii**) It was clarified that electron transfer from Tyr203 to Trp144 is an important step between *A. C. pseudoazurin* and *A. C. nitrite reductase* (Yamaguchi, et al *Biochem. Biophys. Res. Commun.***2005**,*336*,210). **iv**) We also believe that Tyr and Trp are also two first to be oxidized amino acids in processes associated with radiation-induced damages. Clearly, all these features indicate that charge transfer between Tyr and Trp is involved more generally in radical enzymes, ET proteins, and protein damage. All this evidence suggests that Trp with its smallest IP among the residues could be the essential reason for why Trp is frequently involved in many biological ET processes. Thus, we think that IP could be used as an indirect quantity to scale the potential ability of a species in releasing an electron or accepting a hole. Certainly, its ability to be oxidized depends on the oxidation potential of an oxidant (OX) or the IP (or the reduction potential) of the oxidant anion (OX^-) after it gets an electron. Since our

calculations indicate that IPs of α-helices could be smaller than the IP of Trp, when the helices are sufficiently long, we think that the helix C-terminus could participate in hole-hopping migration as an alternative relay when the "normal" charge transport mechanisms that use cofactors and/or metals to tune the redox potentials to transport charge are not available, as experimentally demonstrated by a series of studies of charge transfer along helices, or across different helices, by the Kimura group (see refs 25-28,39-43 in the text).

***b*) *Regarding the Capping Effects*.**

In general, many α-helices are capped in proteins using amino acid residue side-chains, peptide loops, water molecules and other molecular fragments as the capping groups. According to their ionization potentials, all these capping groups for the C-terminus could be classified into three types: positively charged groups such as $-NH_3^+$, $-ArgH^+$, neutral side-chains, loop backbone, and waters. **i**) For the positively charged groups as the C-terminus capping groups, as mentioned in the text and figures below, they can increase IP_v of α-helices, and also forces the ionizable zone of a α-helix to shift inward (toward the N-terminus). **ii**) For water molecules, as demonstrated below (Figures S9, S10), the capping by water molecules hardly affect the IP_v variation regularity along the helix length. **iii**) For loop peptide backbone and the side-chain with amide group as the capping groups, since the peptide unit is same as the backbone unit of α-helices, they can assist the ionization through delocalizing the generated electronic hole by sharing. Thus, they also obey the IP_v-residue number relationship found here. **iv**) If the capping groups are phenol, indole and other aromatic groups which are easily ionized, they can play a role of a relay station to assist hole migration themselves. Their assisting behaviors are similar to that of an indole (the side-chain of Trp (W) residue) linked to helix backbone mentioned in text. That is, when the IP_v of an α-helix with a certain length is smaller than theirs, the generated hole is localized at the C-terminus of the α-helix, while when the IPv of an α-helix is larger than theirs, the hole is trapped at this residue. Of course, if the IP_v of an α-helix is comparable to theirs, they can share the hole with the α-helix C-terminus. **v**) The other side-chain groups basically play an assisting role, but do not affect the IPv-residue number dependence. In addition, regarding capping groups, see Sagermann, M.; Mårtensson, L.; Baase, W.; Matthews, B. *Protein Science* **2002**, *11*, 516–521.

***c*) *Regarding Vertical Ionization Potentials* (IP_v) *of the Natural Helices*.**

To further clarify the dependence of IP_v and spin density distributions of α-helices on the helix chain length, a series of α-helices [α-$(G)_n$, α-$GW(G)_{n-2}$, α-$W(G)_{n-1}$ (n=4-16), α-$G_3W(G)_{n-4}$ (n=8~22), α-LQTWVETWAFSET (PDB 1PJQ) and α-FEQEFQMRVMEEQV (PDB 2QDO), including Trp (W) at different positions] extracted directly from natural structure peptide helices were also employed to determine these energy parameters and spin density distributions by carrying out single point calculations at the UB3LYP/6-31G(d) level of theory. These model α-helices (α-$(G)_n$) were built up by replacing the side-chain by a H, changing the original residue into a Gly residue, while for others a W residue is kept at the required position. The relevant results are given below (Figures S19-S25 and Table S2). These results clearly confirm good agreement in IP_v and spin densities between the optimized modeled helix structures and the wild-type helix structures.

***d*) *Regarding Effects from Twisting and Bending*.**

Actual α-helical proteins are generally bent, twisted or distorted from ideal geometry. Certainly, small degrees of such distortions can not yield large effects on the IP_v~residue number relationship and will not change the trends although some values may be changed slightly. However, if the bending degree or twisting degree are large for a α-helix, this α-helix may be viewed as two α-helices linked by a loop, thus their IP_v~helix length relationship still follows the regularity proposed here.

***e*) *Regarding Correlation of* IP_v *with Dipole Moments*.**

In general, for the α-helices (α-$(G)_n$), even if they are slightly bent or distorted, their dipole moment directions are along their helix axes. Clearly, IP_v are positively linearly correlated with their dipole moments, as shown in Figure 2. Even if a group such as a Trp (W) is linked to a terminus of an α-helix, leading to a deviation of dipole moment direction from its helix axis and value variation, IP_v~dipole moment still exhibits a good linear correlation (Figure 2 for the α-$GW(G)_{n-2}$ series). In fact, if an α-helix is long, the contribution of the dipole moment of the side-chain is relatively too small to deviate the total dipole moment direction from the helix axis. Further, if an α-helix backbone of a peptide chain is surrounded by many other side-chains, forming an arbitrary α-helix polypeptide, the direction of total dipole moment is still close to the helix axis,

because their symmetric distributions around the helix backbone will lead to an overall cancellation effect on the total dipole moment.

Thus, we believe the correlation between IP_v and dipole moment is basically applicable to all α-helices.

3. Some Calculated Data

Table S1. The vertical ionization potentials (IP_v, eV), adiabatic ionization potentials (IP_A, eV), dipole moment (μ, Debye), and energies (eV) of HOMO for α-$(G)_n$, α-$(G)_n$-R, α-$GW(G)_{n-2}$, and α-$GW(G)_{n-2}$-R obtained at the B3LYP/6-31++G(d,p)//B3LYP/6-31G(d) theory of level. W=Trp, Y=Tyr, and M=Met

	n	4	5	6	7	8	9	11	13	15	W	Y	M
α-$(G)_n$	IP_V	8.13	8.02	7.77	7.71	7.61	7.26	7.07	6.87	6.74	7.49	8.09	8.07
	IP_A	7.94	7.70	7.43	7.41	7.30	6.95	6.78	6.59	6.48	7.19	7.50	8.18
	μ	16.28	18.30	22.72	27.08	31.42	37.87	47.62	58.12	68.46	4.79	4.04	2.90
	HOMO	6.23	6.37	5.98	6.08	5.99	5.62	5.45	5.27	5.16	5.83	6.39	6.17
α-$(G)_n$-R	IP_V		10.55		10.05		9.67	9.41	9.18	9.00			
	IP_A		10.27		9.83		9.47	9.24	9.02	8.87			
	μ		6.94		6.44		10.60	12.00	16.83	19.17			
	HOMO		9.06		8.62		8.28	8.04	7.86	7.70			
α-$GW(G)_{n-2}$	IP_V	7.27	7.17	7.13	7.21	7.11	7.07	6.91	6.79	6.70			
	IP_A	6.94	6.86	6.95	6.96	6.98	7.16	6.66	6.58	6.47			
	μ	12.08	16.62	21.80	26.19	32.00	36.57	46.55	56.66	67.24			
	HOMO	5.77	5.83	5.94	5.82	5.73	5.68	5.43	5.28	5.16			
α-$GW(G)_{n-2}$-R	IP_V					8.90	8.80	8.72	8.63	8.52			
	μ					8.32	9.92	9.66	11.35	15.72			
	HOMO					7.31	7.33	7.48	7.46	7.45			

4. Spin Density Distributions and Geometries for all Helices

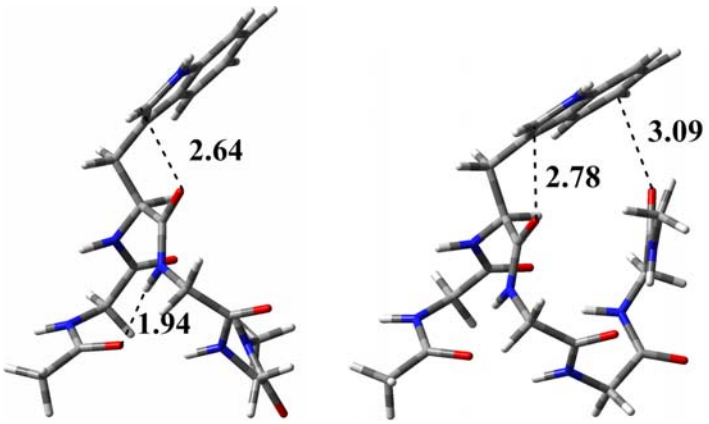

α-GW$(G)_2^{\bullet+}$ α-GW$(G)_3^{\bullet+}$

Figure S1. The geometry structures of α-GW$(G)_2^{\bullet+}$ and α-GW$(G)_3^{\bullet+}$ with main structural parameters.

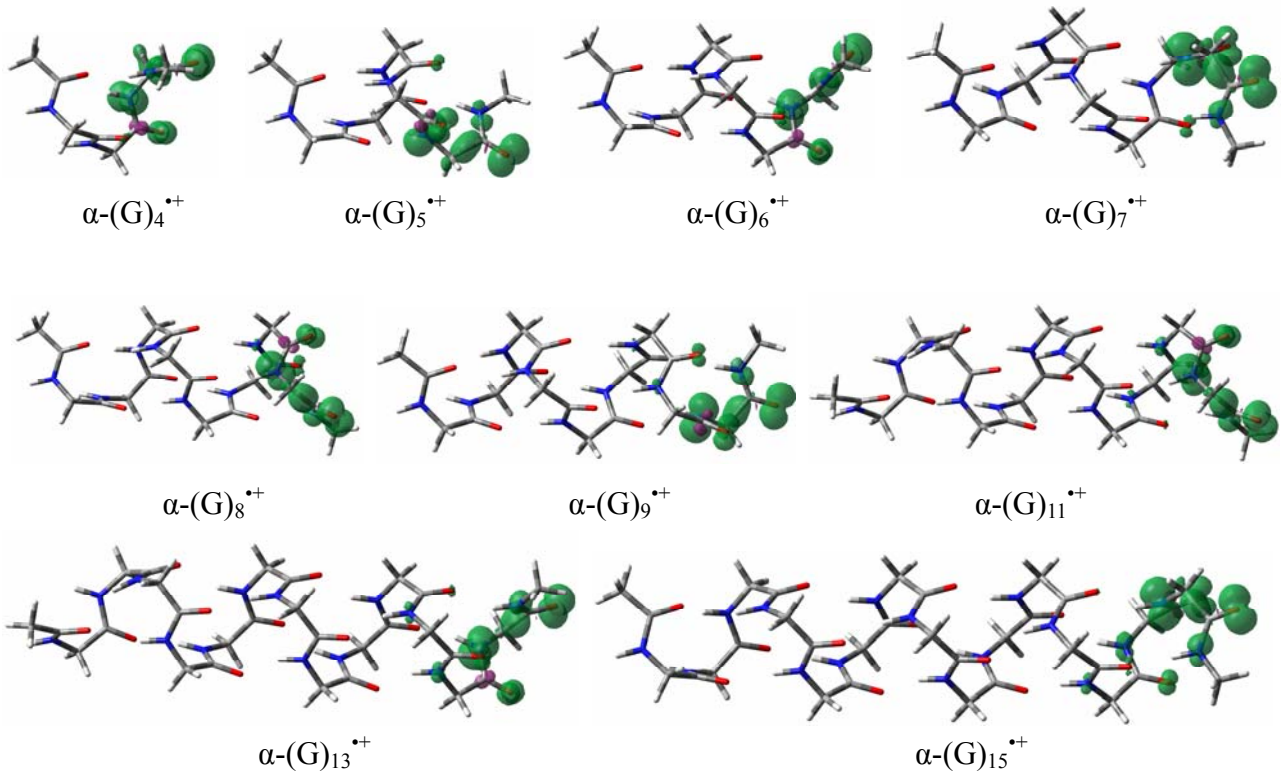

α-$(G)_4^{\bullet+}$ α-$(G)_5^{\bullet+}$ α-$(G)_6^{\bullet+}$ α-$(G)_7^{\bullet+}$

α-$(G)_8^{\bullet+}$ α-$(G)_9^{\bullet+}$ α-$(G)_{11}^{\bullet+}$

α-$(G)_{13}^{\bullet+}$ α-$(G)_{15}^{\bullet+}$

Figure S2. The distribution of the spin densities in the α-$(G)_n^{\bullet+}$ (n=4~15) series.

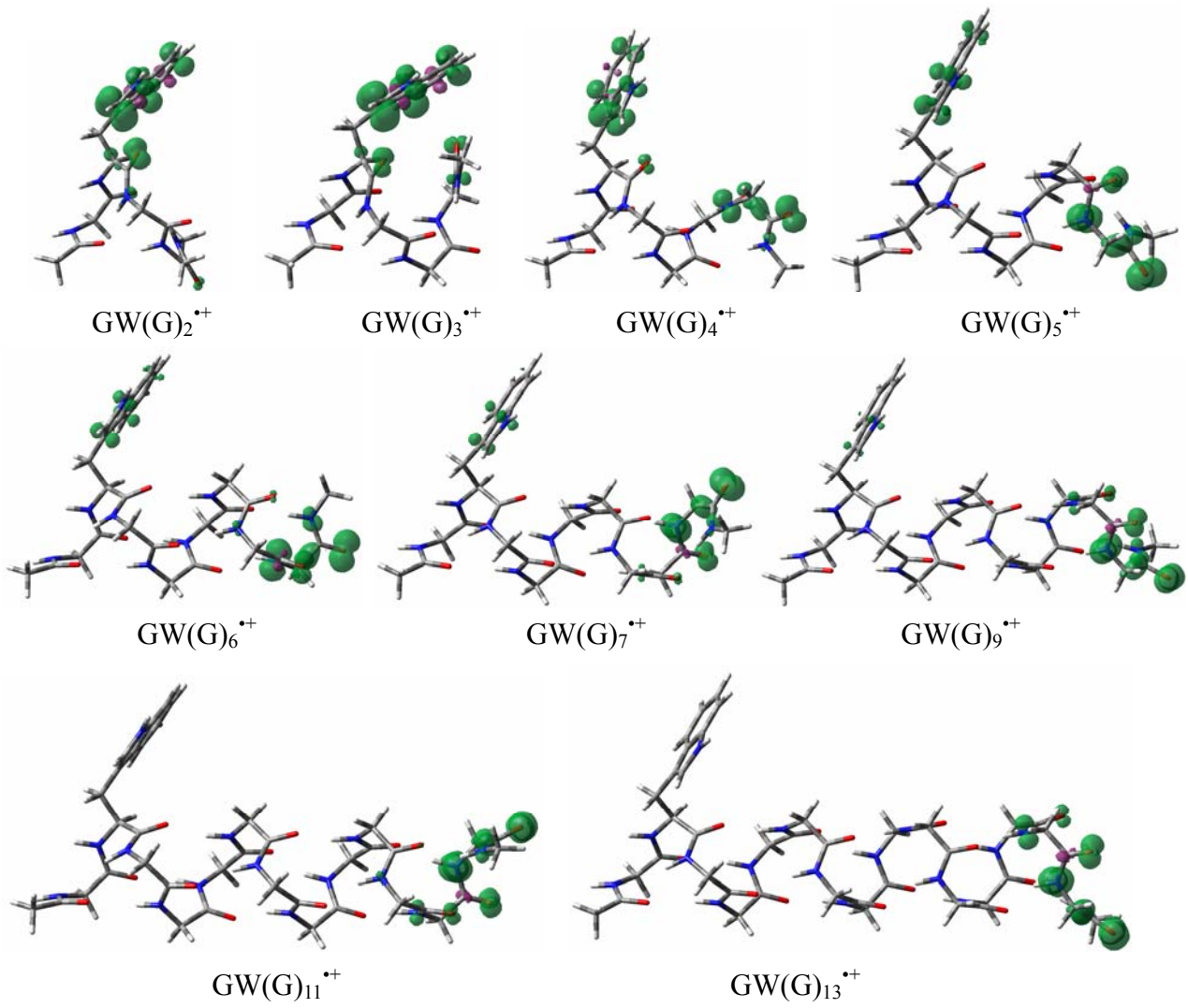

Figure S3. The distribution of the spin densities in the α- $GW(G)_{n-2}^{\bullet+}$ (n=4~15) series.

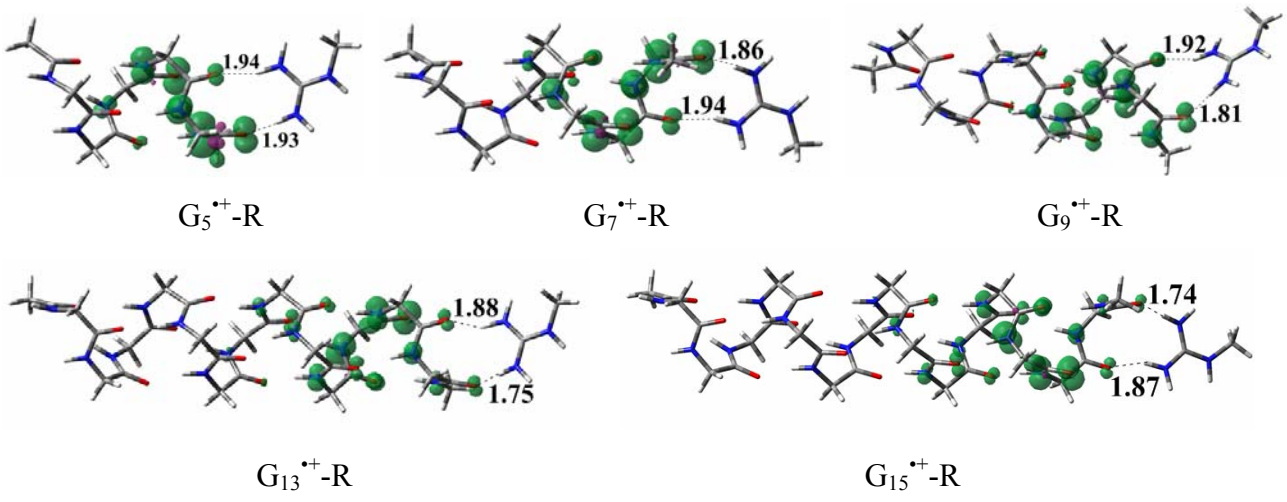

Figure S4. The spin density distribution of α-$G_n^{\bullet+}$-R ("R" represents the methylguanidinium) with main structural parameters.

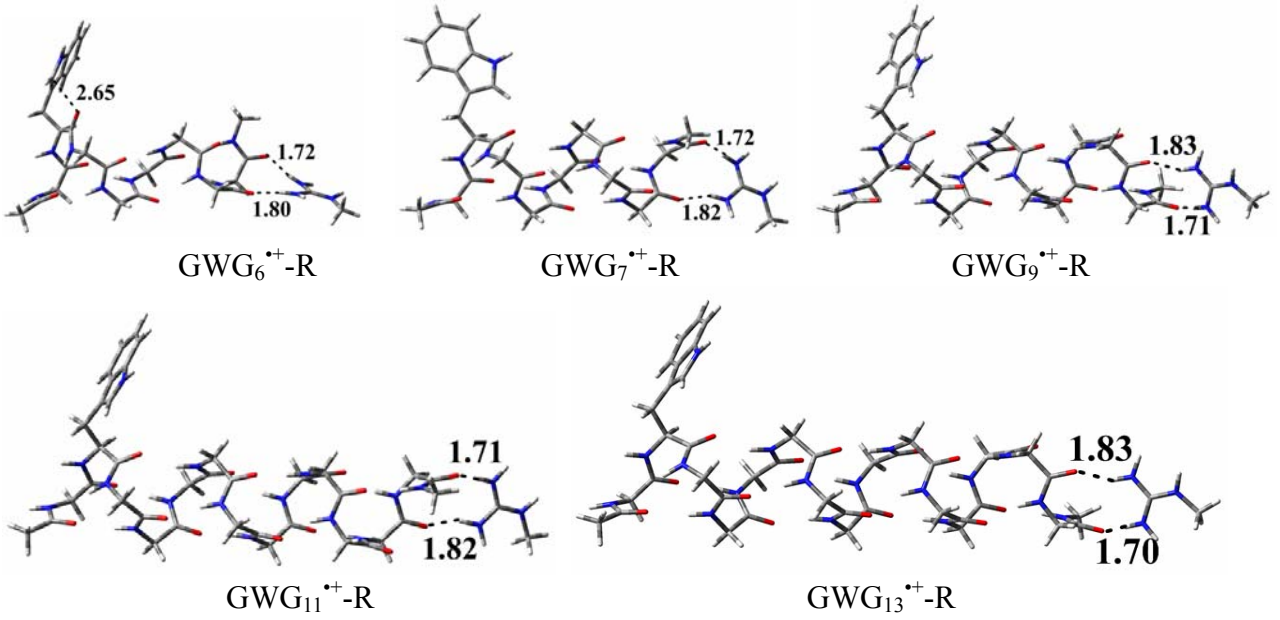

$GWG_6^{\bullet+}$-R $GWG_7^{\bullet+}$-R $GWG_9^{\bullet+}$-R

$GWG_{11}^{\bullet+}$-R $GWG_{13}^{\bullet+}$-R

Figure S5. The geometries of the α-$GW(G)_{n-2}^{\bullet+}$-R (n=8~15) series with main parameters.

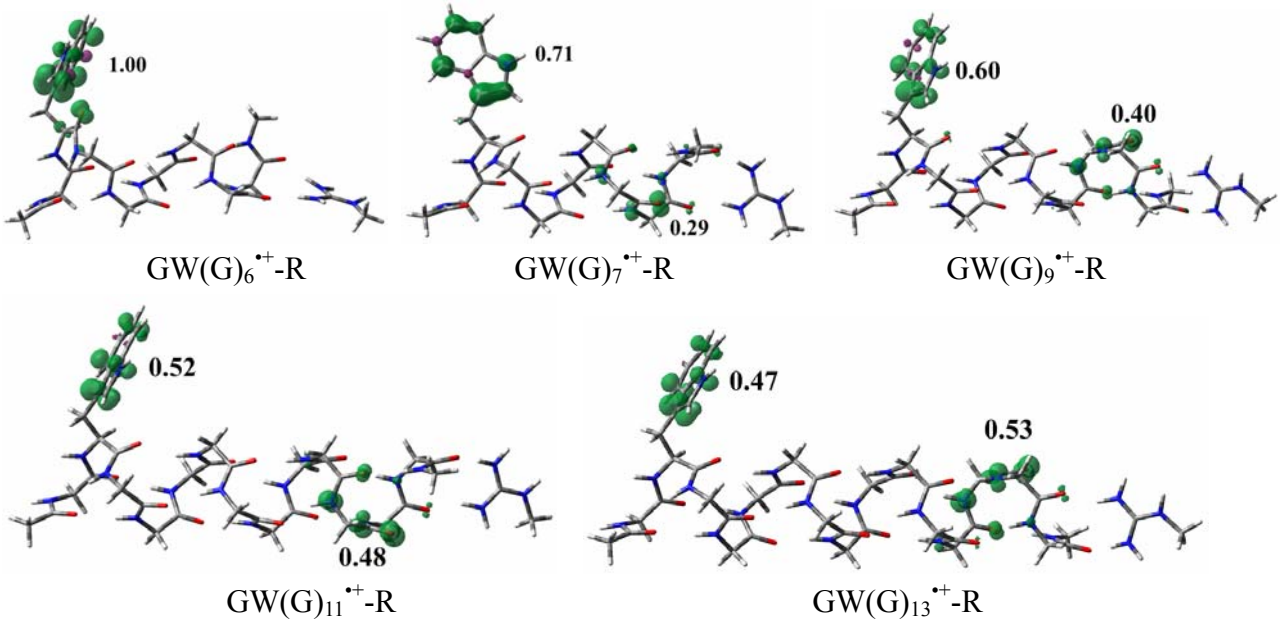

$GW(G)_6^{\bullet+}$-R $GW(G)_7^{\bullet+}$-R $GW(G)_9^{\bullet+}$-R

$GW(G)_{11}^{\bullet+}$-R $GW(G)_{13}^{\bullet+}$-R

Figure S6. The distribution of the spin densities in the α- $GW(G)_{n-2}^{\bullet+}$-R (n=8~15) series.

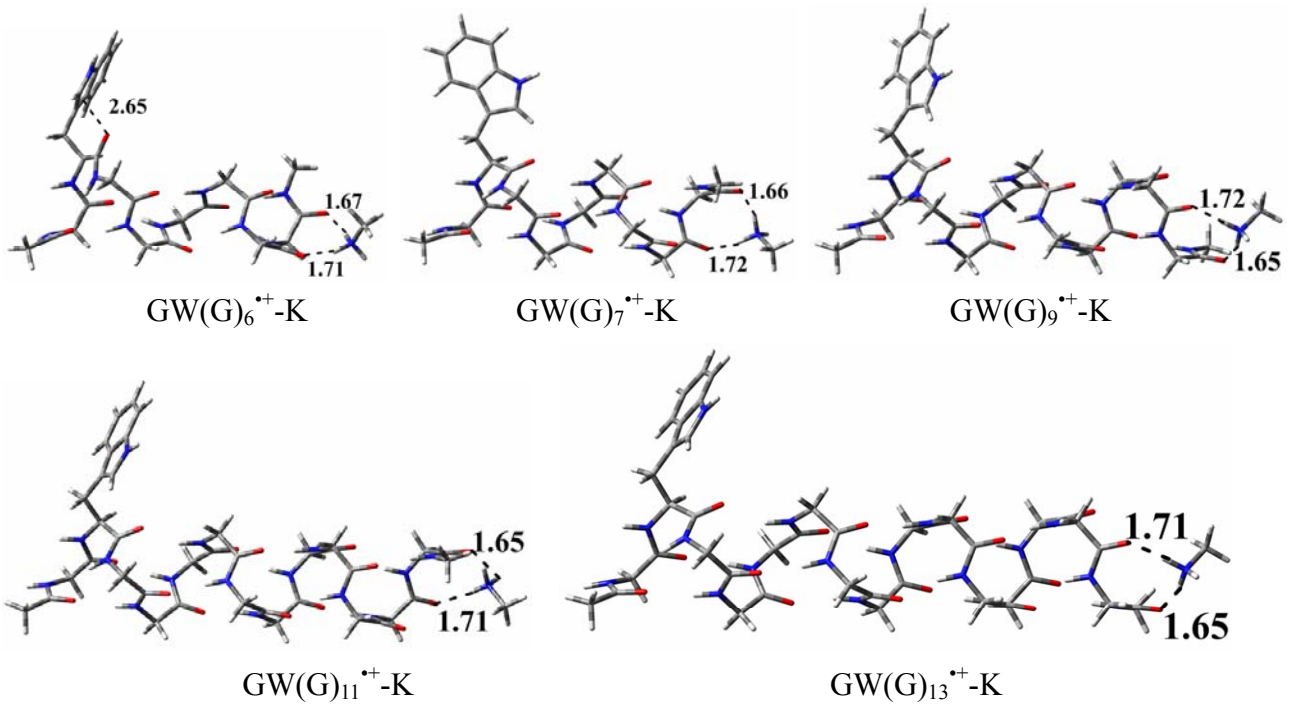

$GW(G)_6^{\bullet+}$-K $GW(G)_7^{\bullet+}$-K $GW(G)_9^{\bullet+}$-K

$GW(G)_{11}^{\bullet+}$-K $GW(G)_{13}^{\bullet+}$-K

Figure S7. The geometries of the α- $GW(G)_{n-2}^{\bullet+}$-K (n=8~15) series with main parameters

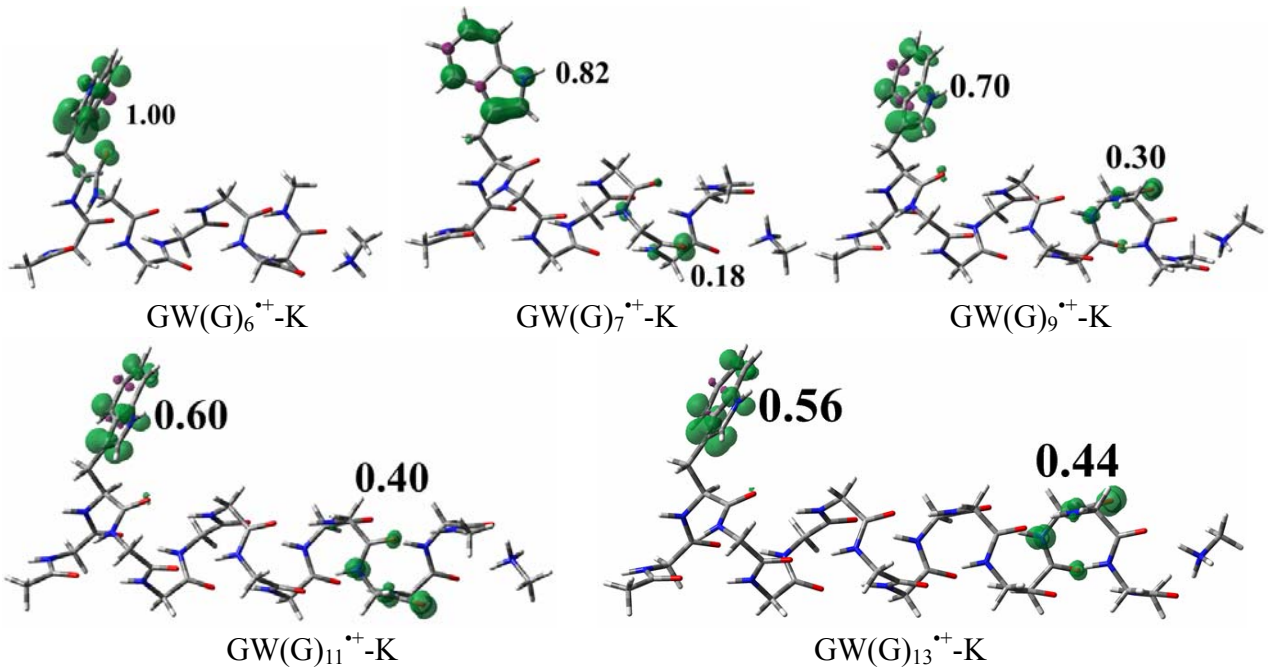

$GW(G)_6^{\bullet+}$-K $GW(G)_7^{\bullet+}$-K $GW(G)_9^{\bullet+}$-K

$GW(G)_{11}^{\bullet+}$-K $GW(G)_{13}^{\bullet+}$-K

Figure S8. The distribution of the spin densities in the α- $GW(G)_{n-2}^{\bullet+}$-K (n=8~15) series.

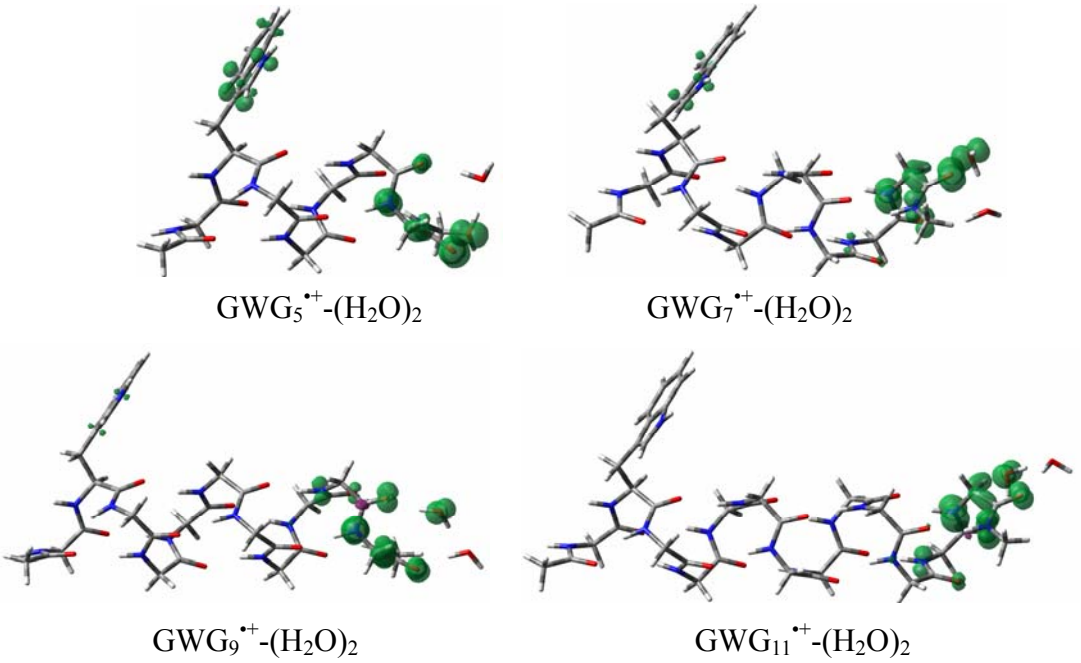

Figure S9. The distribution of the spin densities of $GWG_{n-2}^{\bullet+}$-$(H_2O)_2$ (n=7, 9, 11, 13) changes with the increase of helix length.

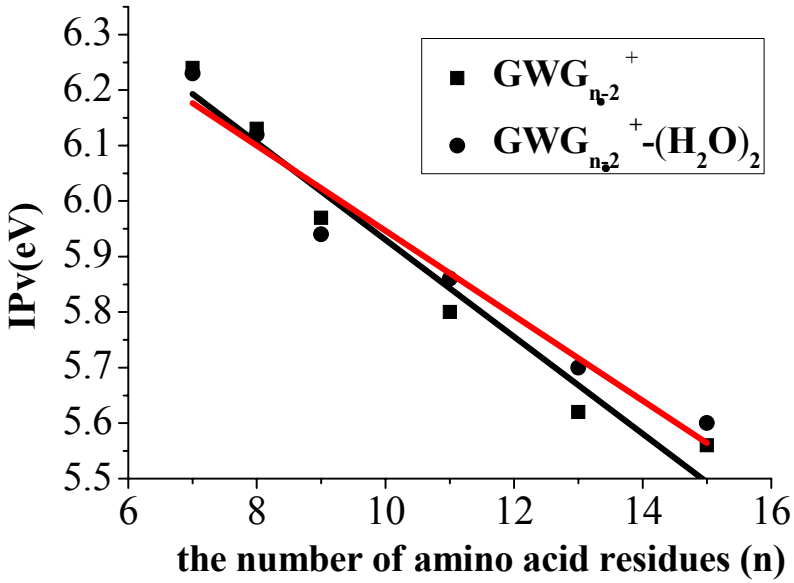

Figure S10. The vertical ionization energies (IP_v) of α-$GW(G)_n^{\bullet+}$ and α-$GW(G)_n^{\bullet+}$-$(H_2O)_2$ (n=7~15) changes with the increase of the number of residues. This indicate that two water molecules in the tail of α-helices affects the vertical ionization energies of α-$GW(G)_n^{\bullet+}$ very slightly.

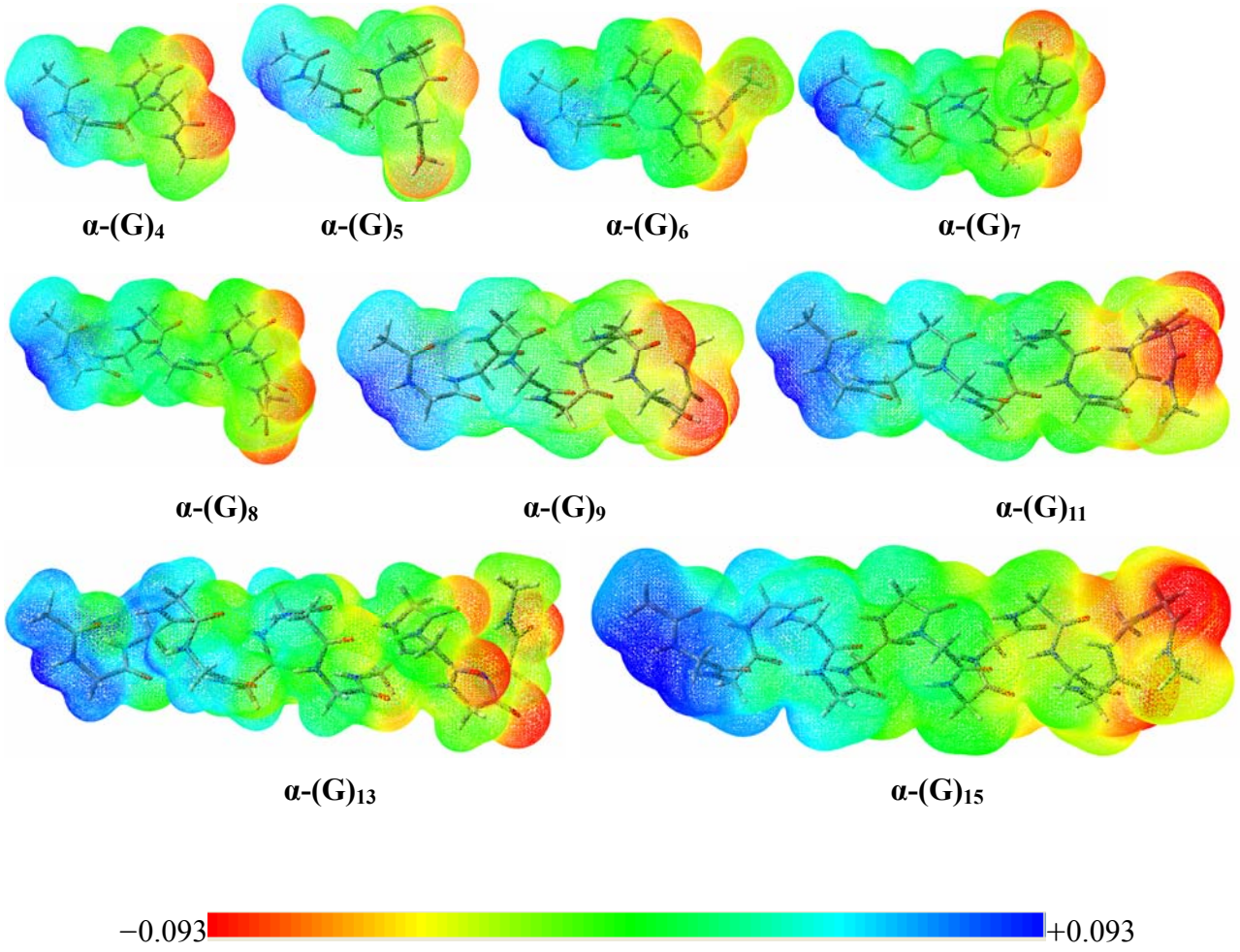

Figure S11. Molecular electrostatic potential surfaces for α-$(G)_n$ (n=4~15), mapped from -0.093 to +0.093 *au*, with a 0.0004 e $Å^{-3}$ isosurface of the electron density.

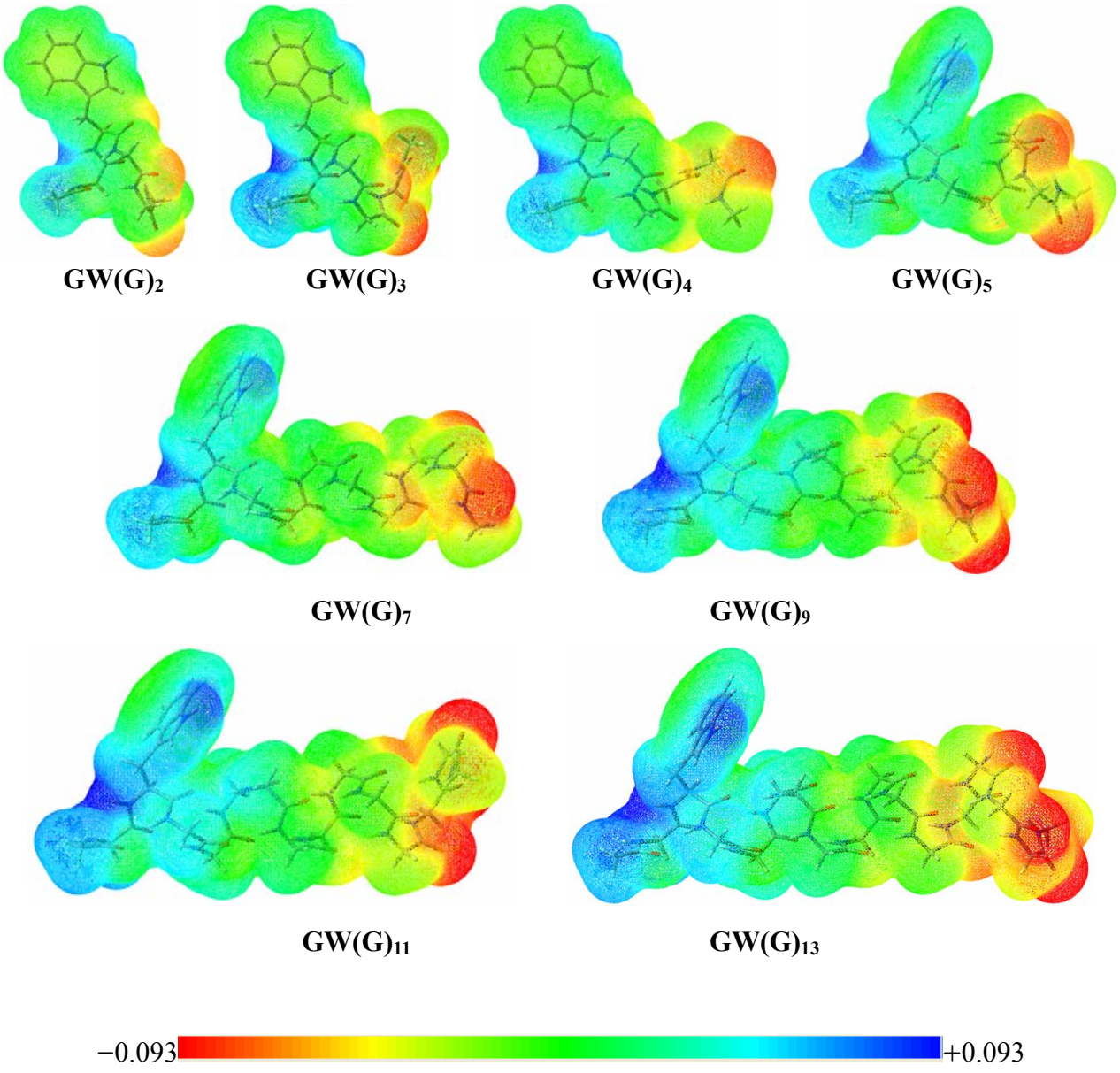

Figure S12. Molecular electrostatic potential surfaces for α-GW(G)$_{n-2}$, mapped from -0.093 to +0.093 *au*, with a 0.0004 e Å^{-3} isosurface of the electron density.

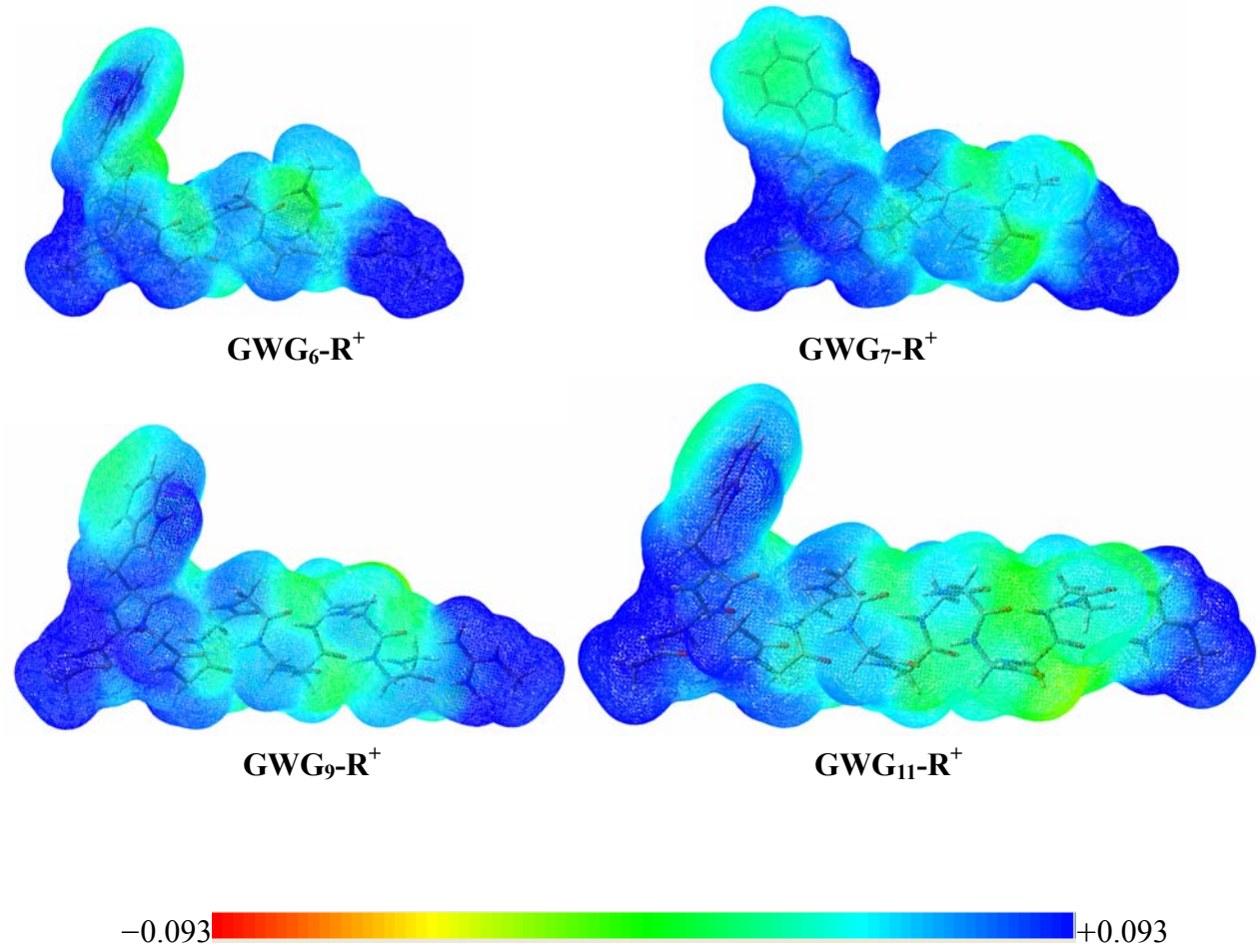

Figure S13. Molecular electrostatic potential surfaces for α-GW$(G)_{n-2}$-R^+, mapped from −0.093 to +0.093 *au*, with a 0.0004 e $Å^{-3}$ isosurface of the electron density.

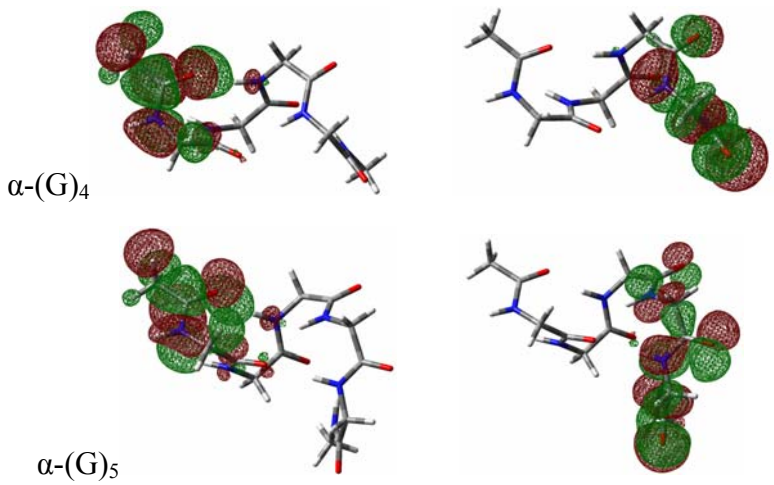

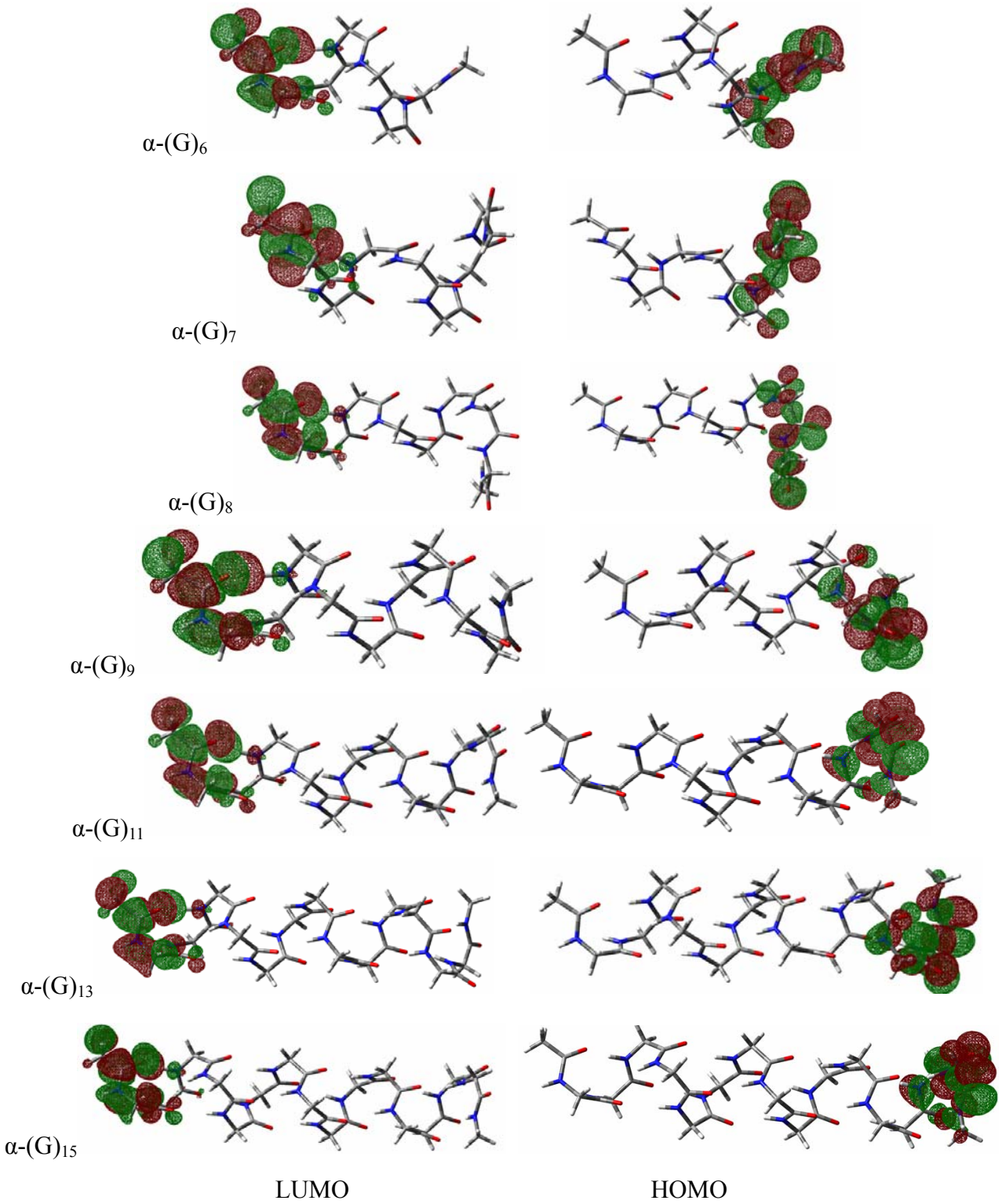

Figure S14 The lowest unoccupied molecular orbitals (LUMO) and the highest unoccupied molecular orbitals (HOMO) for α-$(G)_n$ (n=4~15).

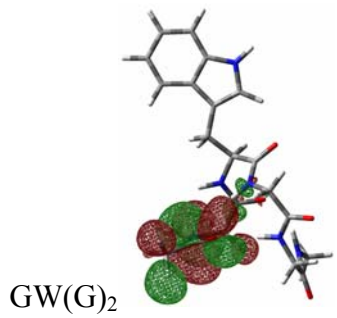
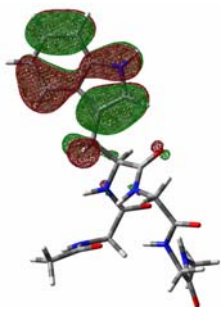

$GW(G)_2$

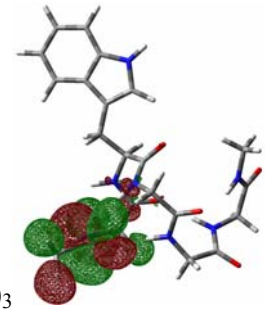
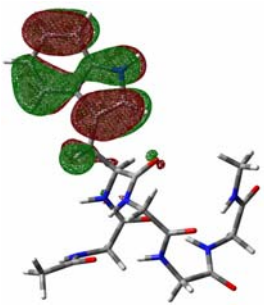

$GW(G)_3$

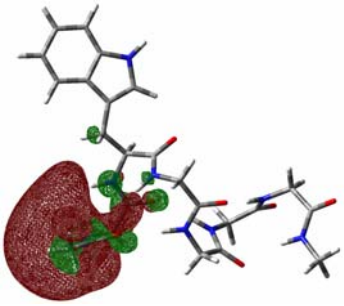
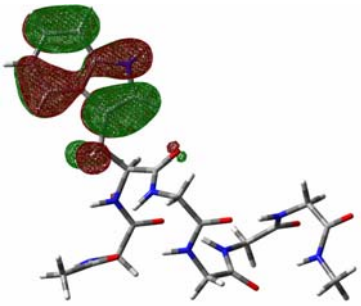

$GW(G)_4$

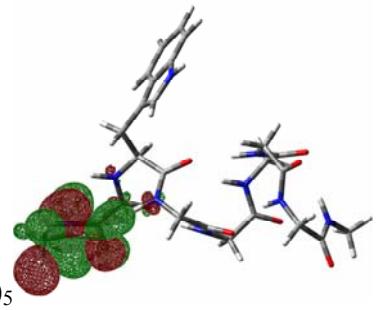
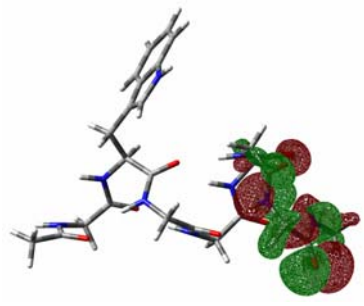

$GW(G)_5$

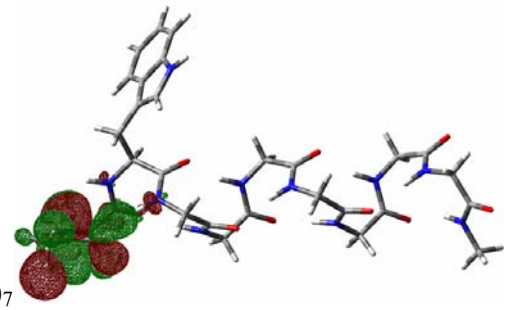
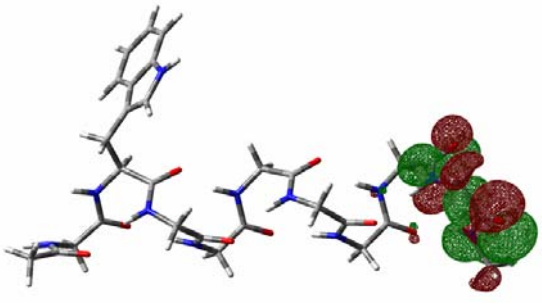

$GW(G)_7$

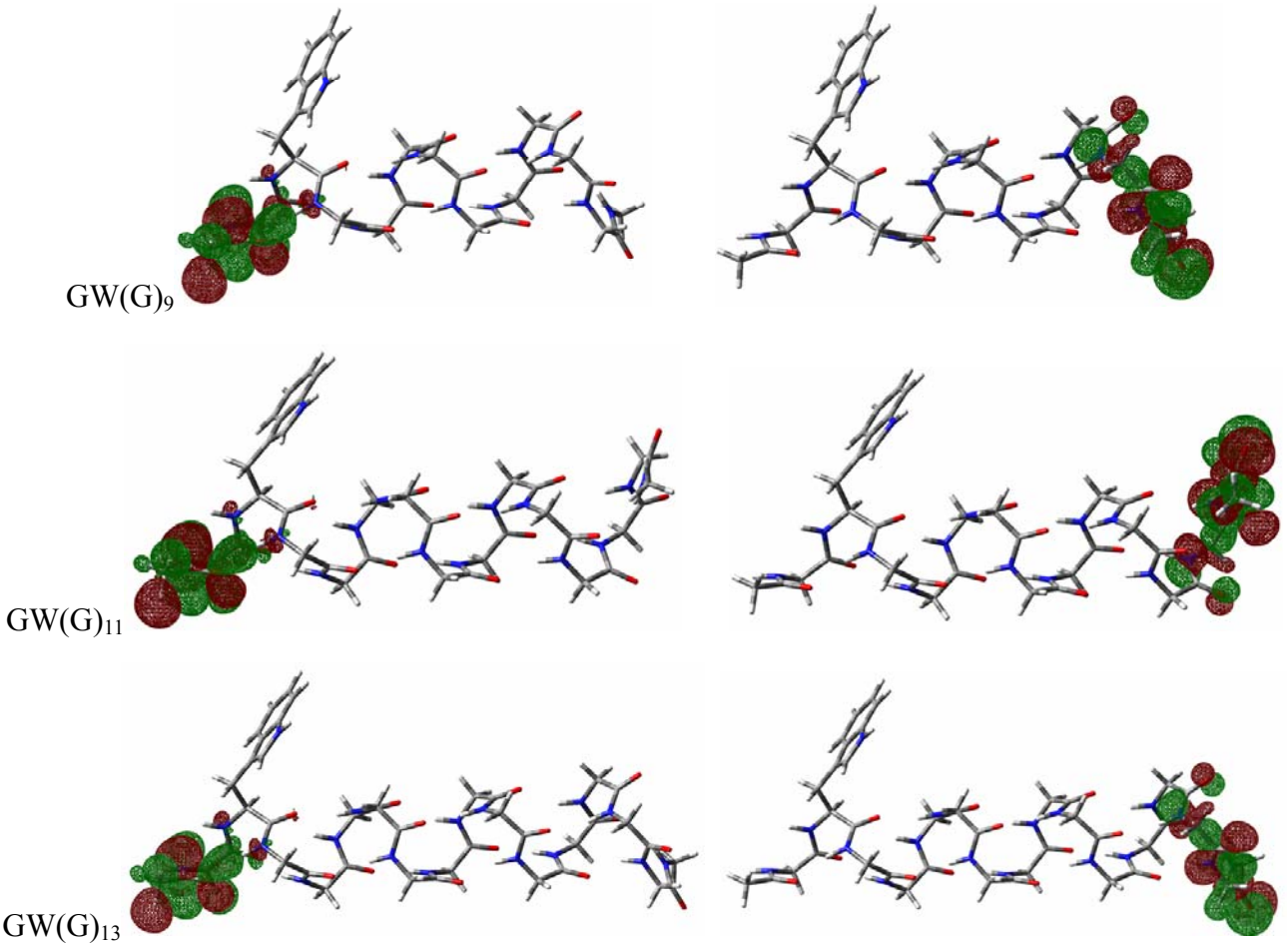

Figure S15. The lowest unoccupied molecular orbitals (LUMO) and the highest unoccupied molecular orbitals (HOMO) for α-GW(G)$_{n-2}$ (n=4~15).

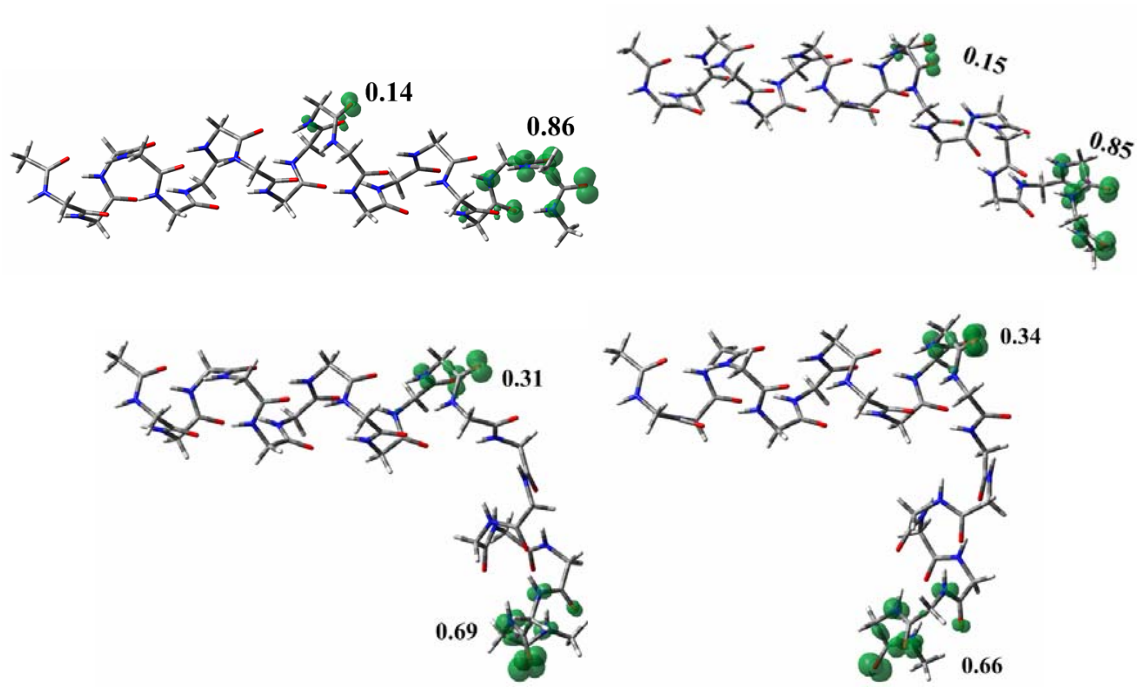

Figure S16. The distribution of spin density changes with the folding or bending of poly-$(G)_{19}$.

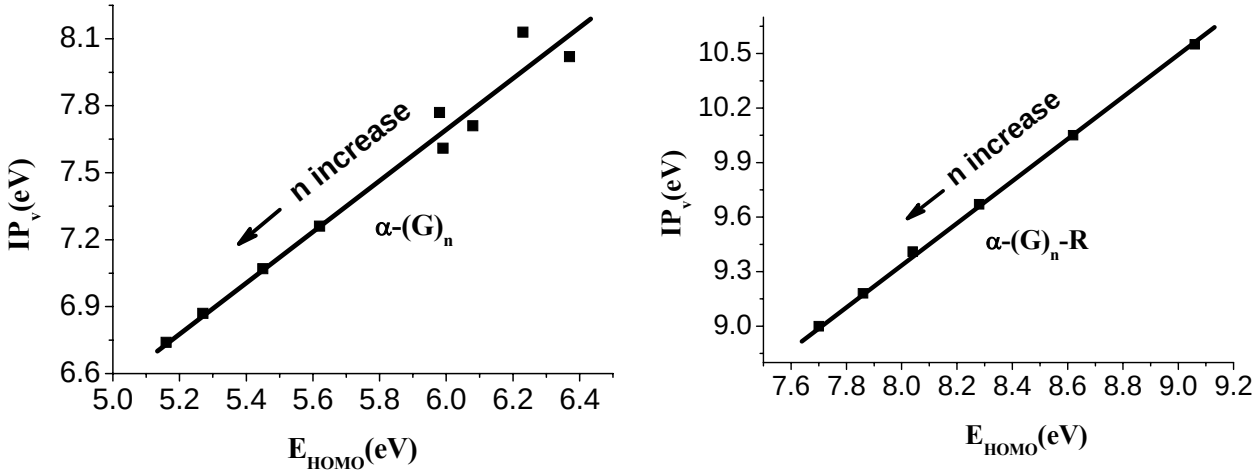

Figure S17. The correlation of the vertical ionization potentials (IP_v) and the HOMO energies for the optimized α-$(G)_n$ and α-$(G)_n$-R systems. These good correlations indicate that increase of the helix length lead to an upshift of HOMO localizing at the helix C-terminus, thus decreasing the vertical IP.

5. Relevant IP_v Data for Natural α-helix Structures

To further clarify the dependence of IP_v and spin density distributions of α-helices on the helix chain length and the position of a W residue, a series of α-helices [α-$(G)_n$, α-$GW(G)_{n-2}$, α-$W(G)_{n-1}$ (n=4-16), α-$G_3W(G)_{n-4}$ (n=8~22), α-LQTWVETWAFSET (1PJQ) and α-FEQEFQMRVMEEQV (2QDO)] extracted directly from natural structure peptide helices were also employed to determine these energy parameters and spin density distributions by carrying out single point calculations at the UB3LYP/6-31G(d) level of theory. The relevant results are given below (Figures S19-S25 and Table S2). These results clearly confirm the good agreement in IP_v and spin densities between the optimized modeled helix structures and the natural wild-type helix structures.

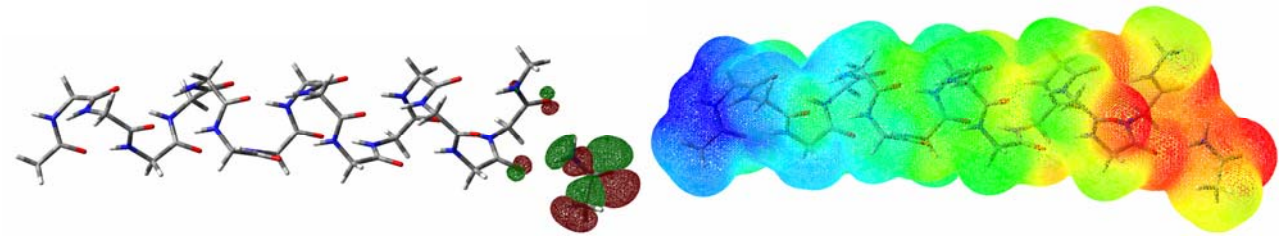

HOMO **EPS**

Figure S18. HOMO and molecular electrostatic potential surfaces for α-$(G)_{16}$-$Q^{\bullet+}$ (the side-chain of glutamine as C-terminal capping), mapped from -0.093 to +0.093 *au*, with a 0.0004 e $Å^{-3}$ isosurface of the electron density.

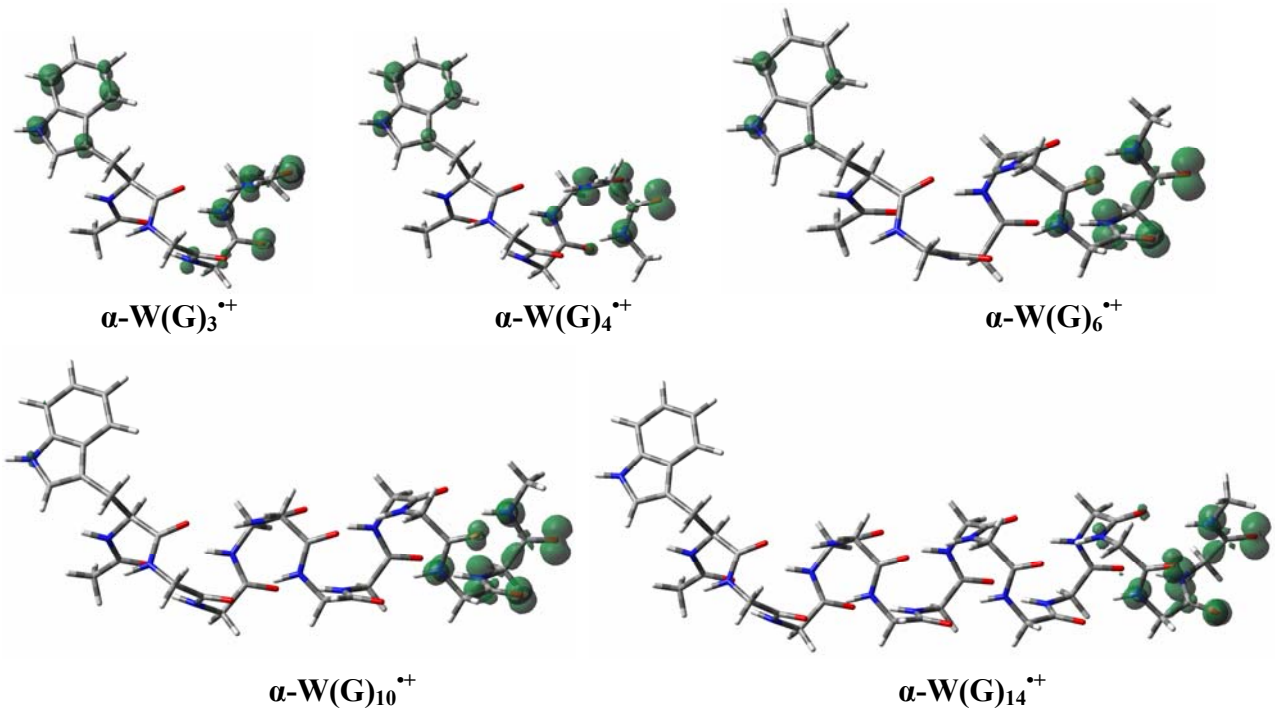

Figure S19. The distribution of the spin densities in the α-GW(G)$_{n-1}^{\bullet+}$ (n=4~16) series (the structures of α-W(G)$_{n-1}$ are extracted from the PDB crystal structure without further optimizations) changes with increase of the number of residues, which is consistent with that of the optimized α-GW(G)$_{n-2}^{\bullet+}$ (n=4~16) series. These results are obtained by carrying out single point calculations at the UB3LYP/6-31G* level of theory.

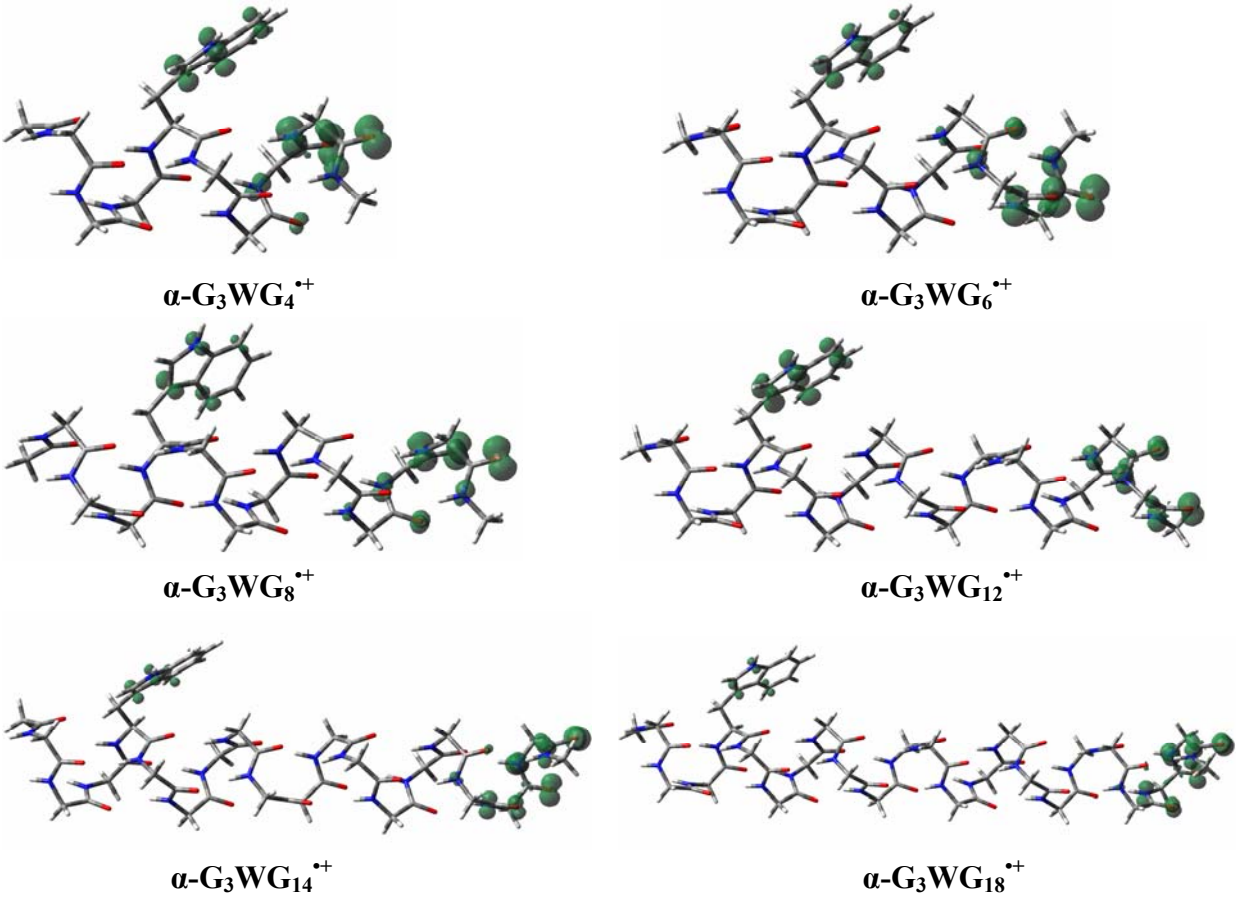

Figure S20. The distribution of the spin densities in the α-$G_3W(G)_{n-4}^{\bullet+}$ (n=8~22) series (the structures of α-$W(G)_{n-1}$ are extracted from the PDB crystal without further optimizations) changes with increase of the number of residues, which is consistent with that of the optimized α-$GW(G)_{n-2}^{\bullet+}$ (n=4~16) series. These results are obtained by carrying out single point calculations at the UB3LYP/6-31G* level of theory.

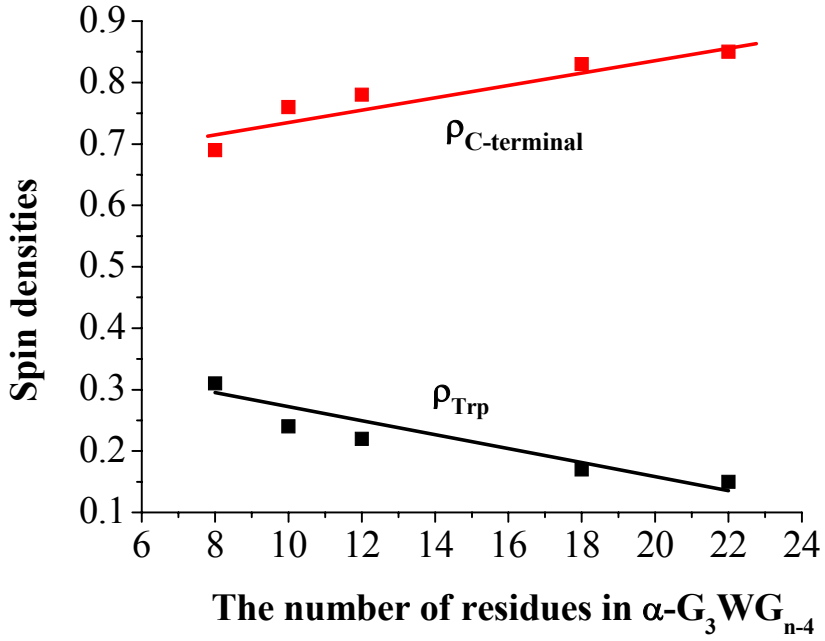

Figure S21. The spin density (ρ) distributions change with the increasing number of residues in α-GW(G)$_{n-2}^{\bullet+}$ series (the structures of α-G$_3$W(G)$_{n-4}^{\bullet+}$ (n=8~22) are extracted from the PDB crystal without further optimizations). It is clearly shown that the tendency of the change of ρ at the Trp segment or the C-terminus is consistent with the results of the optimized α-GW(G)$_{n-2}^{\bullet+}$ (n=4~15).

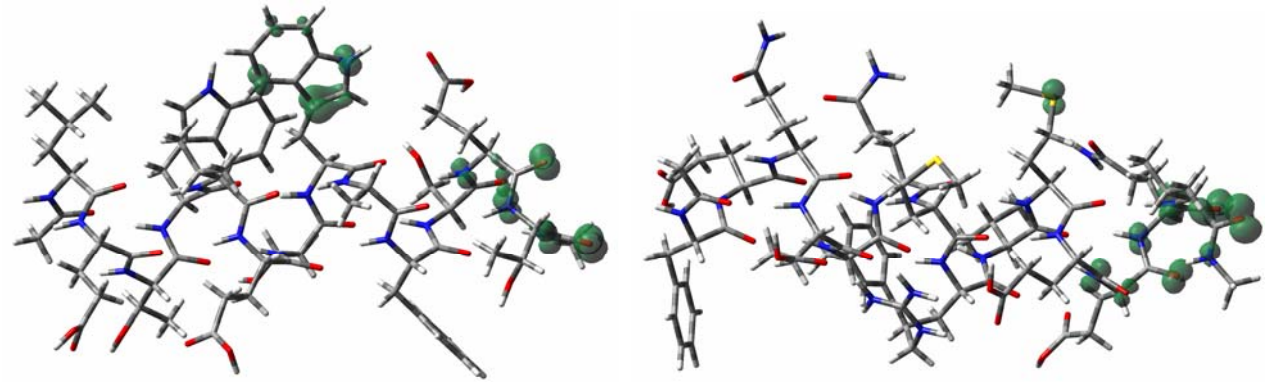

α-LQTWVETWAFSET$^{\bullet+}$ (1PJQ 104-116) α-FEQEFQMRVMEEQV$^{\bullet+}$ (2QDO 14-27)

Figure S22. The position of electronic hole was examined in the real α-helices. α-LQTWVETWAFSET was taken out of 1PJQ (PDB, from residue 104 to residue 116) and α-FEQEFQMRVMEEQV is taken out of 2QDO (PDB, from residue 14 to residue 27). It is clear that the electronic hole mainly resides at the C-terminal of α-helices. These results are obtained by carrying out single point calculations at the UB3LYP/6-31G* level of theory.

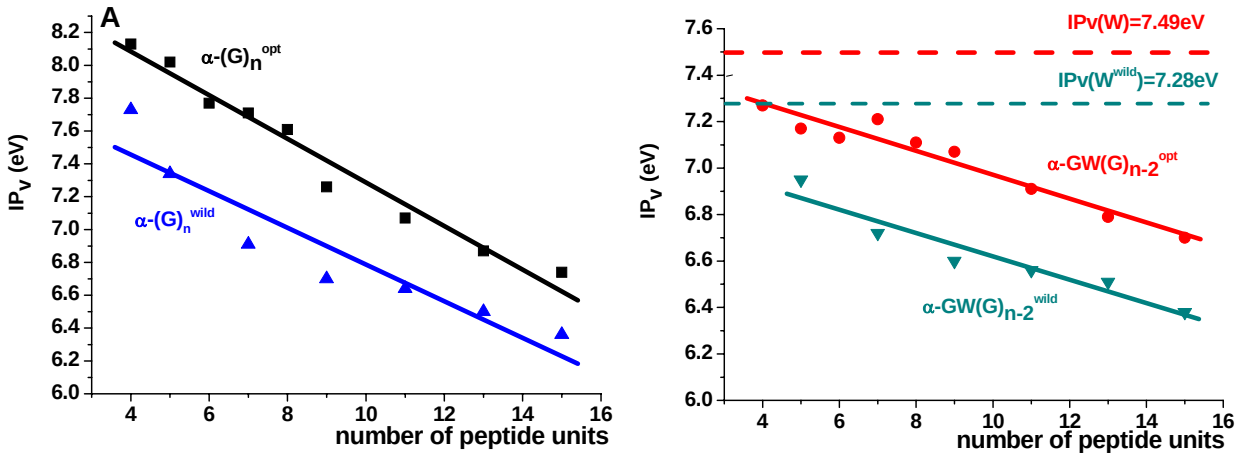

Figure S23. (***A***, ***left***) shows that the tendency of vertical ionization potentials (IP_v) for α-$(G)_n^{opt}$ and α-$(G)_n^{wild}$ changes with the increase of amino acid residues. (***B***, ***right***) shows that the tendency of vertical ionization potentials (IP_v) for α-$GW(G)_{n-2}^{opt}$ and α-$GW(G)_{n-2}^{wild}$ changes with the increase of amino acid residues. The superscript "opt" denotes that the results are obtained by carrying out B3LYP/6-31++G(d,p)//B3LYP/6-31G(d) calculations and the superscript "wild" means that the results are obtained by carrying out B3LYP/6-31++G(d,p) calculations without optimizations on the structures directly extracted from Protein Data Bank (PDB) crystals. Clearly, the two lines are nearly parallel, indicating that the changing tendency of optimized α-helix with the increase of amino acid residues is well consistent with that of the wild-type α-helix.

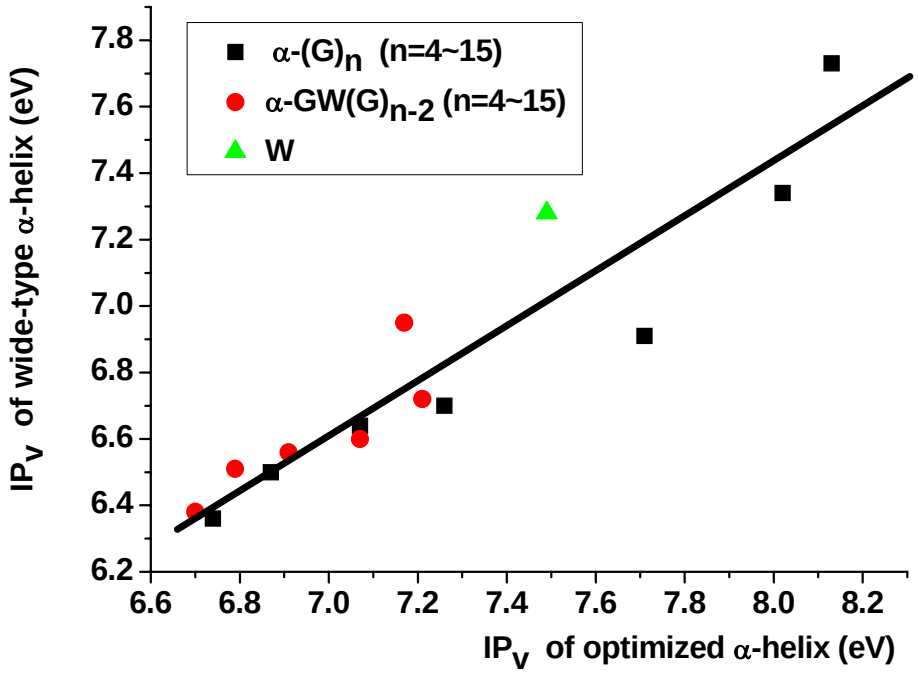

Figure S24. The linear correlation between IP_v of the optimized α-helix and IP_v of the wild-type α-helix [α-helix including all the (α-$(G)_n$ and α-$GW(G)_{n-2}$ series (n=4~15), "W" denotes a tryptophan residues.].

Table S2. Comparison between the vertical ionization potentials (IP_v, in eV) for the α-$(G)_n^{opt}$, α-$(G)_n^{wild}$, α-$GW(G)_{n-2}^{opt}$, and α-$GW(G)_{n-2}^{wild}$ obtained at the B3LYP/6-31++G(d,p) theory of level. The data are used in the above figures.

IP_V(eV)	4	5	6	7	8	9	11	13	15	W
α-$(G)_n^{opt}$	8.13	8.02	7.77	7.71	7.61	7.26	7.07	6.87	6.74	7.49[a]
α-$(G)_n^{wild}$	7.73	7.34		6.91		6.70	6.64	6.50	6.36	7.28[b]
α-$GW(G)_{n-2}^{opt}$	6.94	6.86	6.95	6.96	6.98	7.16	6.66	6.58	6.47	
α-$GW(G)_{n-2}^{wild}$		6.95		6.72		6.60	6.56	6.51	6.38	

Notes: "a" denotes that the IP_v of tryptophan residues (W) is obtained by carrying out B3LYP/6-31++G(d,p)//B3LYP/6-31G(d) calculations and 'b" denotes that the IP_v of tryptophan residues (W) is obtained by carrying out the B3LYP/6-31++G(d,p) calculations without structural optimizations.

6. Surrounding Medium Effect

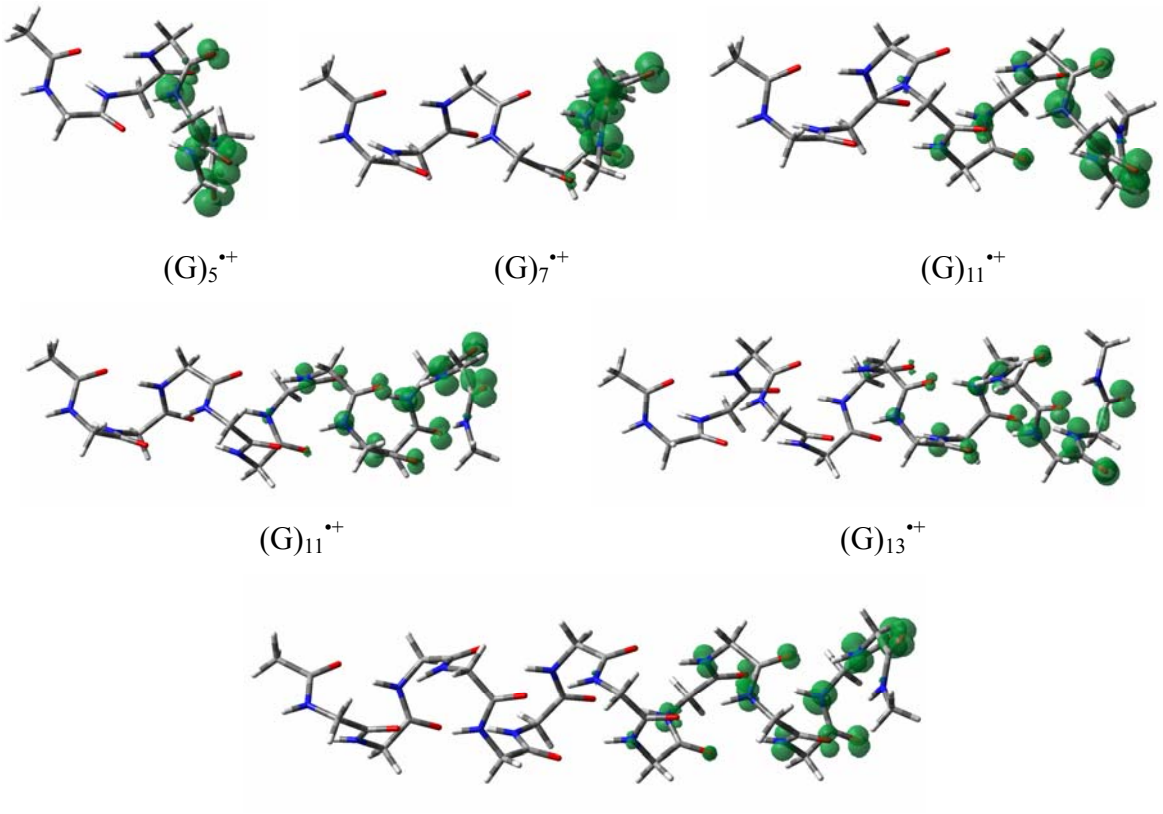

Figure S25. Positions of a hole in α-$(G)_n^{\bullet+}$ with the structures of optimized neutral helixes are determined in water (ε=78.36) by using the polarizable continuum model with a single-point B3LYP/6-31++G(d,p) calculation.

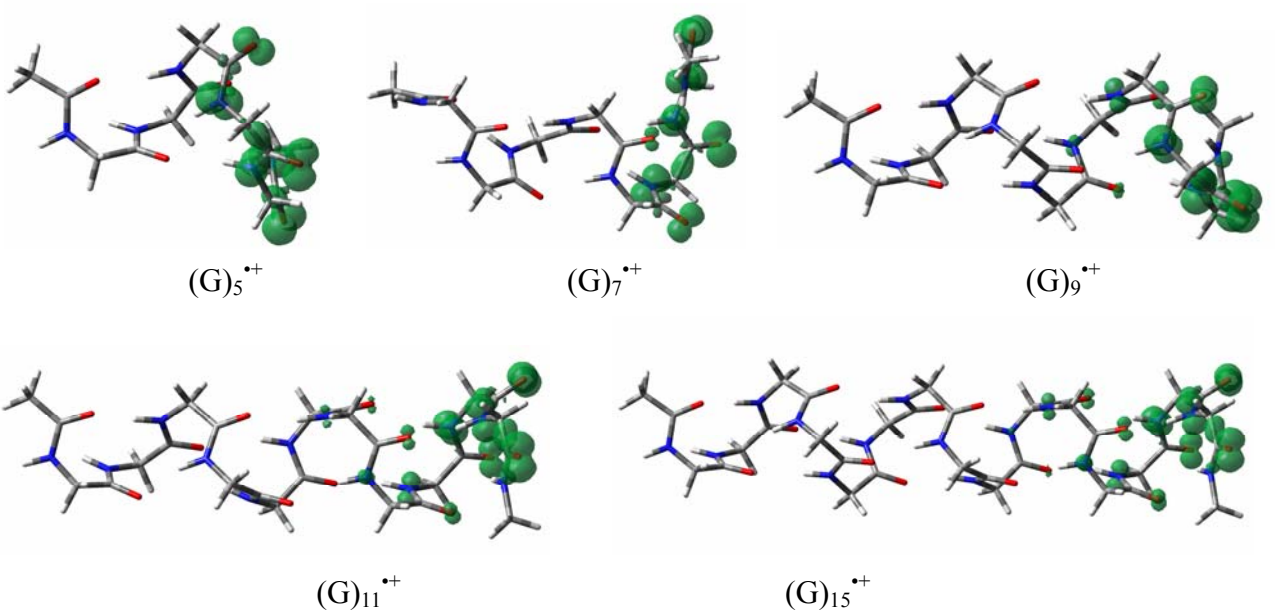

Figure S26. Positions of a hole in α-$(G)_n^{\bullet+}$ with the structures of optimized neutral helixes are determined in water (ε=2.247) by using the polarizable continuum model with a single-point B3LYP/6-31++G(d,p) calculation.

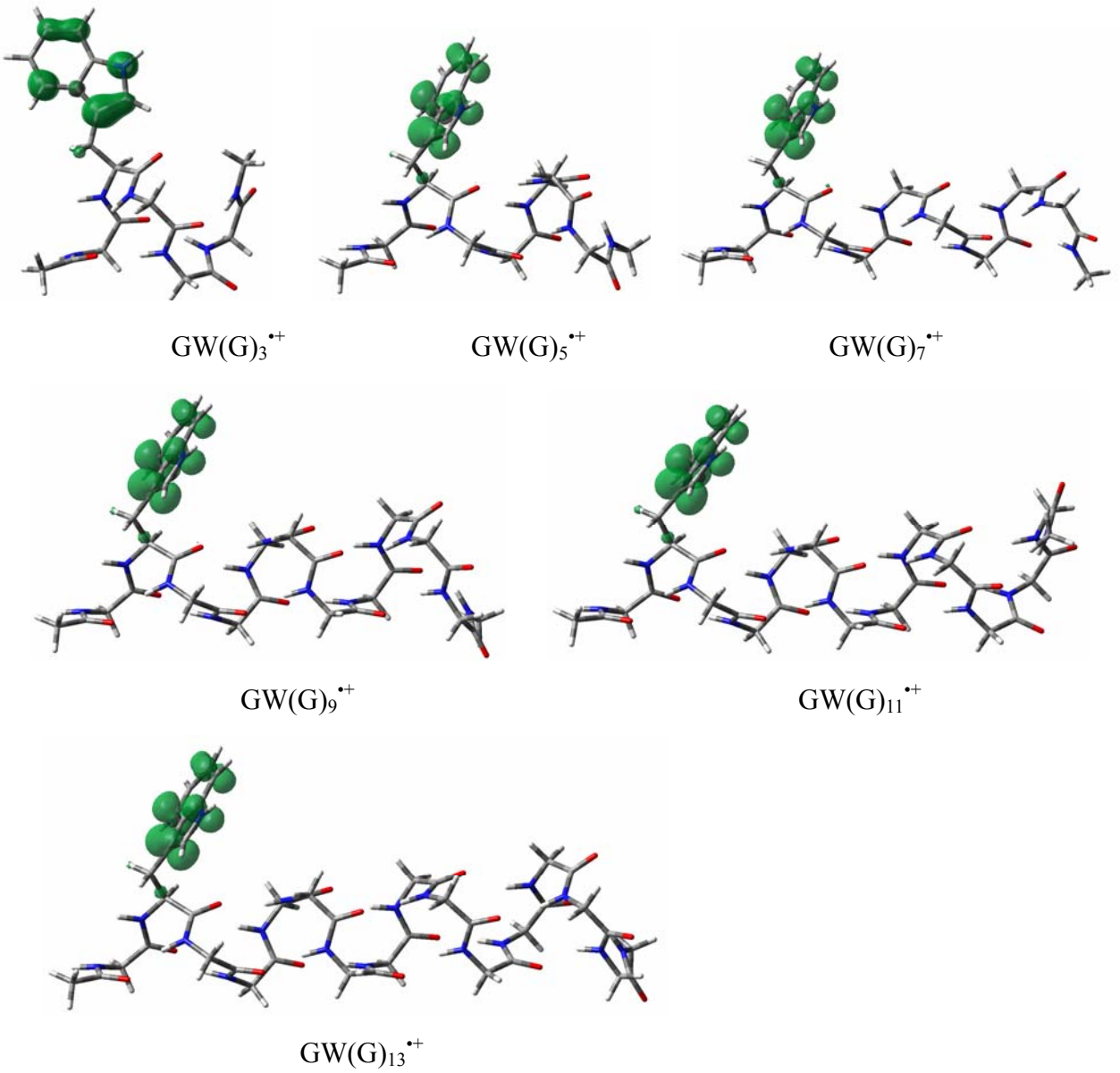

Figure S27. Positions of a hole in α-GW(G)$_{n-2}^{\bullet+}$ with the structures of optimized neutral helixes are determined in water (ε=78.36) by using the polarizable continuum model with a single-point B3LYP/6-31++G(d,p) calculation.

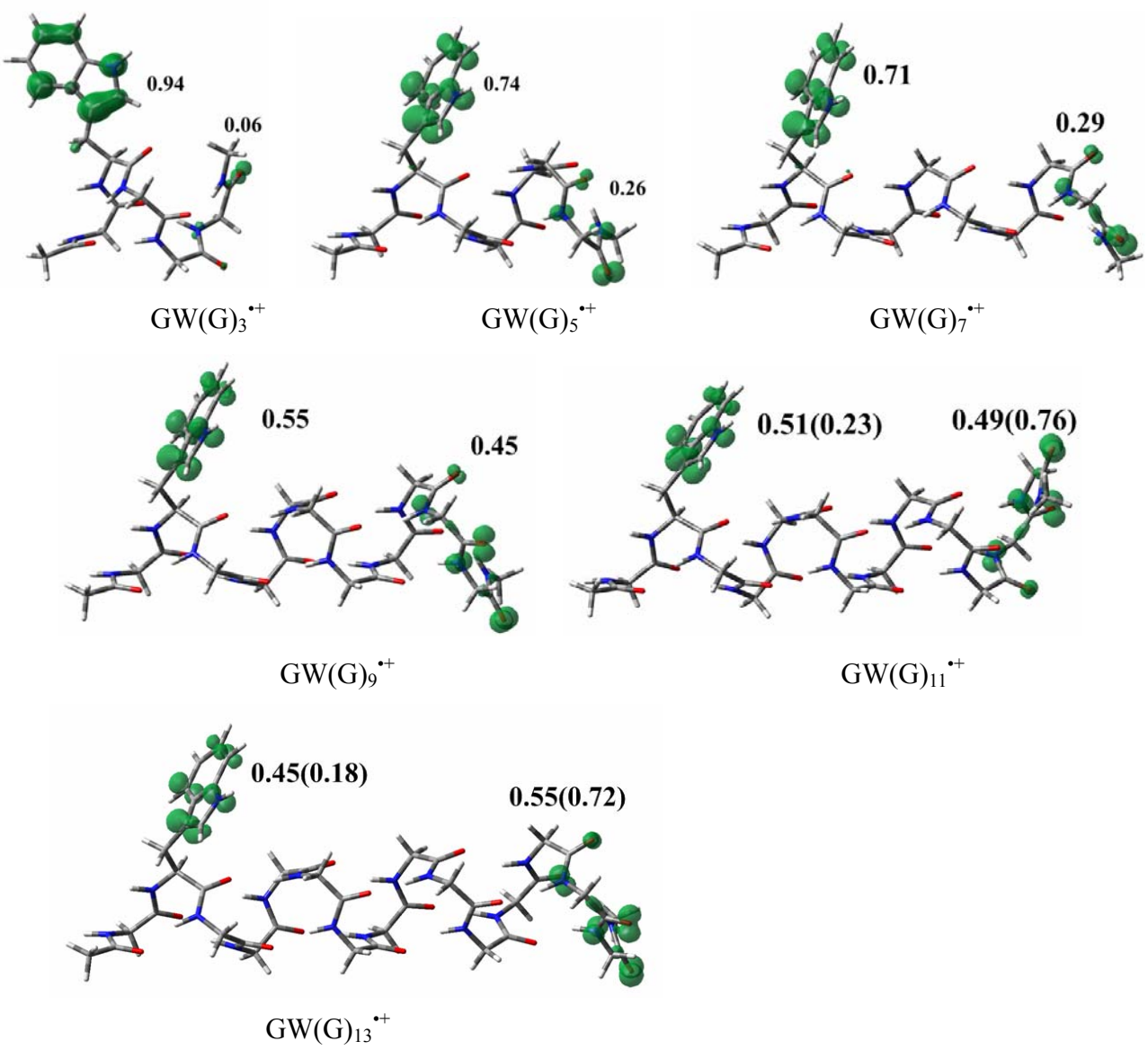

Figure S28. Positions of a hole in α-GW$(G)_{n-2}^{\bullet+}$ with the structures of optimized neutral helixes are determined in water (ε=2.247) by using the polarizable continuum model with a single-point B3LYP/6-31++G(d,p) calculation. The numbers are the amounts of spin densities on the corresponding groups and the numbers in bracket are results after relaxation.

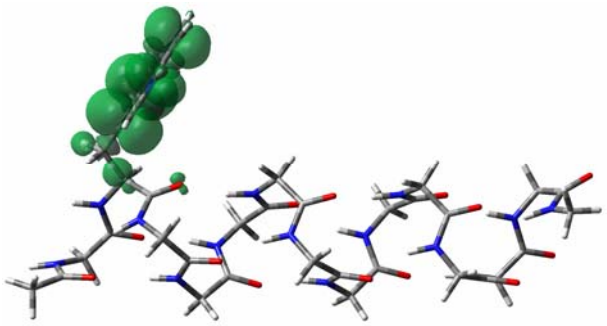

Water (ε=78.36)

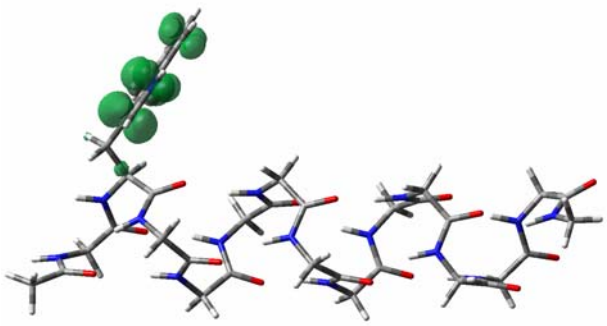

Dichloroethane (10.36)

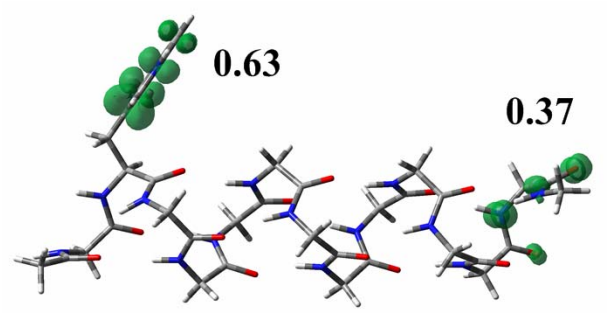

Chlorobenzene (ε=5.621)

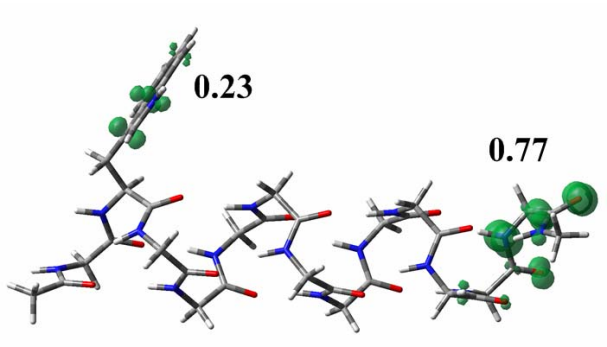

Benzene (ε=2.247)

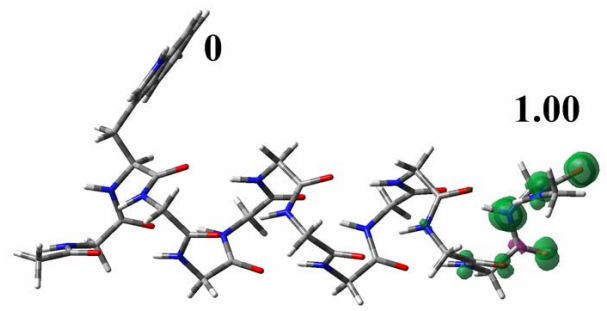

In the gas phase

Figure S29. Position of a hole of α-$GWG_{11}^{\bullet+}$ varies with the different solvents which have different dielectric constants. This change indicates that the formation of a hole in the C-terminus of α-helix may be regulated by the polarity of the dielectric surrounding in proteins.

Table S3. The vertical ionization potentials (IP_v, eV) and dipole moment (μ, Debye) of α-$(G)_n$ obtained at the B3LYP/6-31++G(d,p)//B3LYP/6-31G(d) level of theory in different media (gas phase, water and benzene) with the polarizable continuum model.

α-$(G)_n$		4	5	6	7	8	9	11	13	15	W
Gas phase	IP_V(eV)	8.13	8.02	7.77	7.71	7.61	7.26	7.07	6.87	6.74	7.49 7.51
	IP_A(eV)	7.94	7.70	7.43	7.41	7.30	6.95	6.78	6.59	6.48	7.19 7.20
	μ(Debye)	16.28	18.30	22.72	27.08	31.42	37.87	47.62	58.12	68.46	4.79
Water Benzene	IP_V(eV)		7.03 7.44		7.02 7.20		6.97 7.04	6.95 6.95	6.92 6.80	6.91 6.74	
Water Benzene	μ (Debye)		23.04 20.21		32.91 30.81		45.07 40.96	55.62 51.08	66.94 62.00	78.05 72.70	

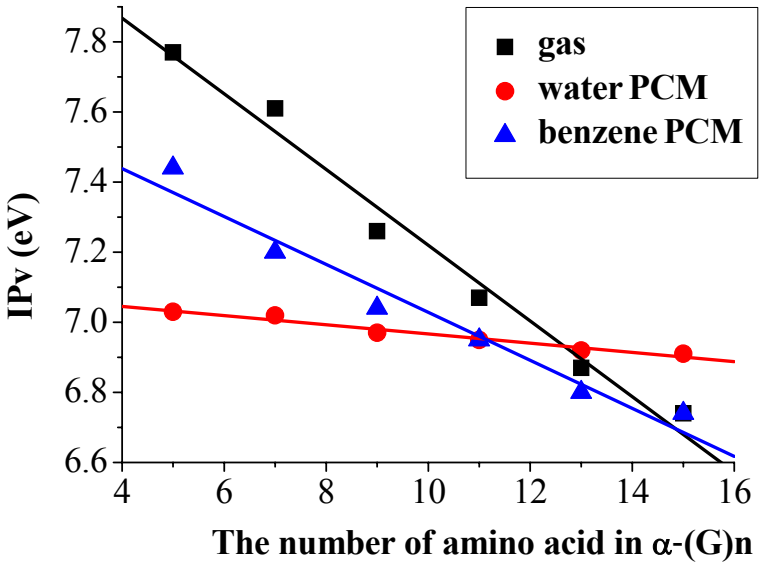

Figure S30. A comparison of the vertical ionization potentials (IP_v, in eV) in the gas phase and different continuum solvents is shown at the B3LYP/6-31++G(d,p)//B3LYP/6-31G(d) level with the polarizable continuum model (PCM).